Synthesis and Characterization of Perovskite Structured Ceramic Membranes for Selective Transportation of Hydrogen Ions

A dissertation submitted in partial fulfillment
of the requirements for the degree of

Master of Philosophy

in

"Inorganic/Analytical Chemistry"

by

KHALID MAHMOOD

Islamabad

Department of Chemistry

Quaid-i-Azam University
Islamabad
2010

DECLARATION

This is to certify that this dissertation entitled **"Synthesis and Characterization of perovskite structured ceramic membranes for selective transportation of hydrogen ions."**. submitted by **Mr. Khalid Mahmood** is accepted in its present form by the Department of Chemistry, Quaid-i-Azam University, Islamabad, Pakistan, as satisfying the dissertation requirements for the degree of *Master of Philosophy in Analytical/Inorganic Chemistry.*

Supervisor:

Prof. Dr. M. Mazhar
Department of Chemistry
Quaid-i-Azam University
Islamabad.

External Examiner:

Dr. Uzaira Rafique
Associate Professor
Department of Environmental Chemistry
Fatima Jinnah Women University
The Mall Rawalpindi.

Head of Section:

Prof. Dr. Amin Badshah
Department of Chemistry
Quaid-i-Azam University
Islamabad.

Chairman:

Prof. Dr. Saqib Ali
Department of Chemistry
Quaid-i-Azam University
Islamabad.

بسم الله الرحمن الرحيم

IN THE NAME OF ALLAH
THE BENEFICIENT, THE MERCIFUL

DEDICATED

TO

MY LOVING PARENTS

ACKNOWLEDGEMENTS

ABSTRACT

Proton conducting solid oxide ceramic membranes of the type $La_{1.0}Ce_{0.8}Y_{0.2}O_x$ (1), $Ba_{1.0}Ce_{0.8}Y_{0.2}O_x$ (2) and $Sr_{1.0}Zr_{0.8}Y_{0.2}O_x$ (3) have been synthesized by the solution method and characterized by FT-IR, TGA and the nature of crystalline products were determined by powder X-ray diffraction analysis. Thermogravimeteric analysis proved that all the materials were oxygen deficient. Surface morphology was characterized by SEM and elemental composition by EDX. The electrical conductivities as a function of the temperature of all the membranes were recorded using the Keithley electrical conductivity meter.

All the samples (1), (2) and (3) were found to be single phase with the crystallite size 17nm, 33nm, and 43 nm respectively. Presence of proton defects in all membranes and their electrical non-conducting or insulating behavior make them suitable for their possible technological applications in solid oxide fuel cells.

CONTENTS

LIST OF TABLES

LIST OF FIGURES

LIST OF ABBREVIATIONS AND NOTATIONS

acac	2, 4-pentanedionate
acacH	2, 4-pentanedione
dmae	N, N-dimethylaminoethanolate
dmaeH	N, N-dimethylaminoethanol
TFA	Triflouroacetic acid
THF	Tetrahydrofuran
EDX	Energy Dispersive X-ray
SEM	Scanning electron microscopy
TGA	Thermogravimetric analysis
FT-IR	Foriour transform infra red spectroscopy
XRD	X-ray diffraction
ICDD	International council for diffraction data
CVD	Chemical vapour deposition
$V_O^{\bullet\bullet}$	Oxygen vacant sites
$OH_O^{\bullet}$	Proton defects
O_O^X	Structural oxygen atoms

It was previously studied that the solid oxide fuel cells are green source of energy. It consumes wet hydrogen as a fuel and produce heat and electricity as a useful energy and water vapours as a by product which are environment friendly. But it is not commercialized due to certain hindrances. The main hindrance is the high cost and complex preparatory methods for the preparation of solid oxide fuel cell components. A typical fuel cell consists of the three components i.e, anode, cathode and electrolyte. The main objective of the research is to prepare the perovskite ceramic electrolyte membranes for solid oxide fuel cell by some efficient method. For this purpose the solution method has been adapted which is a novel method for the preparation of fuel cell components at relatively low temperature.

CHAPTER 1
INTRODUCTION

1. The perovskite structure materials

The first perovskite mineral was discovered by the geologist *Gustav Rose,* in the Ural Mountains in 1839[1] who named it after the famous Russian mineralogist *Count Lev Aleksevich von Perovski.* Now it is the most abundant solid phase (70-80 %) of the lower earth mentle and is one of the most frequently encountered structures in solid-state inorganic compound [2].

The general structure of the perovskite mineral is ABO_3. The ABO_3 perovskite crystal structure is formed by the B cations filling 25% of the octahedral holes in the cubic close-packed AO_3 array [3] as shown in the Fig 1. In the idealized cubic unit cell of such a compound, type 'A' atoms sit at cube corner positions (0, 0, 0), type 'B' atoms sit at body centre positions (1/2, 1/2, 1/2) and oxygen atoms sit at face centered positions (1/2, 1/2, 0).
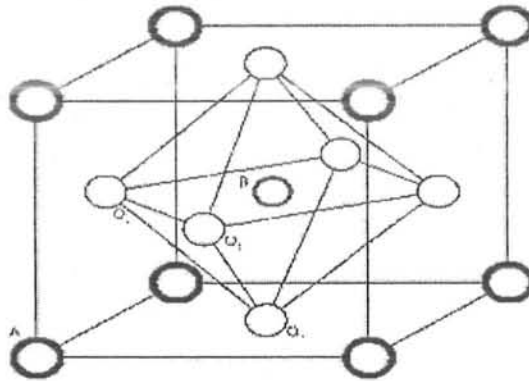
Figure 1: An Ideal perovskite cubic structure

In such a cubic structure, the coordination numbers of the A and B cations are 12 and 6, respectively i.e, each A cation is coordinated to twelve oxide ions and each B cation is coordinated to six oxide ions. If structure become distorted then the coordination number of cations A and B changes and lowers from the ideal case for which the relative ion size matters too much and any slight distortion can produce several lower-symmetry distorted crystal systems, in which the coordination numbers of A cations, B cations or both are reduced, e.g, tilting of the BO_6 octahedra reduces the coordination number of A site cation from 12 to as low as 8. Conversely, off-centering or sliping

from the centre of a B site cation within its octahedron allows it to attain a stable bonding pattern in several perovskite structured ceramic materials.

Complex perovskite structures contain two different B-site cations. This results in the possibility of ordered and disordered perovskites. The orthorhombic and tetragonal phases are the most common in non cubic perovskites. The complex perovskites are produced by doping of B site cation with another metal cation having oxidation state lower than or equal to that of B cation due to which oxygen vacancies in the material are produced which are important characteristic for the proton conducting ceramic electrolyte membranes. In the isovalent perovskite materials the doping of B site cation with the metal of same valence state produces the vacancies not due to imbalance of valence state but due to distortion produced by the difference in the ionic radii of the two metals doping and being doped respectively.

There are certain preliminary mathematical tools which are used to determine the stability, degree of cubicness and degree of distortion in the perovskite materials. These factors are briefly described .

Goldschmidt [4] in early 1920s, proposed a factor which is called as "**tolerance factor**" given by the formula

$$t = (R_A + R_o)/\sqrt{2}(R_B + R_o)$$

Where R_A is the ionic radius of A, R_B is the ionic radius of B, and R_O is the ionic radius of oxygen atom. Geometrically, for an ideal perovskite structure, the ratio of bond length of A---O to B---O bond, is $\sqrt{2}:1$. if the value of t is close to 1, the structure is expected to adapt the ideal cubic symmetry. When the value of t is 0.74 or less and the radius value of the A site ion is smaller than ideal, the BO_6 octahedra will tilt in order to fill space and hence a distorted structure will be obtained. Stable perovskite structures have values approximately $0.75 < t < 1.05$. The tolerance factor however, is based on the ionic radius and should only be used as an estimate because perovskites are not exclusively ionic. The distorted perovskites occur in somewhere wider range of t .this tolerance factor has widely used to determine the formation of perovskite structure and is highly successful in this regard. Most of the researchers use this factor for the determination of stability of the perovskites as a preliminary mathematical tool.

The Jahn-Teller distortion theorem states that a nonlinear molecule cannot be stable in a degenerate electronic state and must undergo distortion in order to break down the degeneracy and become stable[5]. Distortion caused by the Jahn-Teller effect in perovskites usually involves four of the octahedral bonds contracting and two of the octahedral bond lengthening which gives an elongated octahedral shape. e. g, perovkites containing cations such as Cu^{2+} and Mn^{3+} in their octahedral cation site tend to exhibit distortions caused by the Jahn-Teller effect.

2. Properties of the perovskites

Materials containing more than one type of metals are found to display high complexity in structure and diversity in properties. There is a variety of ceramics, which have important applications in the field of optoelectronics, telecommunications, next generation computer memories, infrared detectors, pyrodetectors, gas sensors, catalysis, fuel bells, superconductors and garnets. Perovskite oxides also exhibit a large variety of properties due to the diversity in their structural and chemical composition. Few important properties of perovskites are given in the Table: 1

Table 1. Properties of perovskite oxides

Typical property	Typical compound
Ferromagnetic property	$BaTiO_3$, $PdTiO_3$
Piezoelectricity	$Pb(Zr, Ti)O_3$, $(Bi, Na)TiO_3$
Electrical conductivity	ReO_3, $SrFeO_3$
Superconductivity	$La_{0.9}Sr_{0.1}CuO_3$
Magnetic property	$LaMnO_3$
Ion conductivity	$CaTiO_3$
Catalytic property	$BaCuO_3$

On the basis of electron and ion conductivity ceramic perovskite membranes are used as electrolyte in the **solid oxide fuel cells (SOFC)** to convert the chemical energy of fuel into the electrical energy.

A fuel cell is essentially a battery that does not need recharging. As long as hydrogen and oxygen fuel supplied, it continue to supply heat and an electrical current. It generates electricity inside a cell through reactions between a fuel and an oxidant. The reactants flow into the cell, and the reaction products flow out of it, while the electrolyte remains within it. Fuel cells can operate virtually continuously as long as the necessary flows are maintained.

Fuel cells are thermodynamically open systems because they consume the fuel from an external source and reaction products also leave the system and always have to be refilled [6] while those of the batteries are close system in which reactant and products remain inside the particular boundaries of the battery.

There are several types of the fuel cells depending upon the type of the electrolyte used in the cell. The major types of the fuel cells are, Metal hydride fuel cell, Electro-galvanic fuel cell, Direct formic acid fuel cell, Zinc air battery, Microbial fuel cell, Regenerative fuel cell, Direct borohydride fuel cell, Alkaline fuel cell, Direct methanol fuel cell, Reformed methanol fuel cell, Direct-ethanol fuel cell, Phosphoric acid fuel cell, Molten carbonate fuel cell, Protonic ceramic fuel cell, Direct carbon fuel cell. Protons conducting ceramic solid oxide fuel cells are important among all because of certain reasons which are described below.

Solid oxide fuel cell (SOFC) is a source of clean and efficient power generation to alleviate environmental burdens because they use up the hydrogen as fuel which combines with oxygen to produce water which is environment friendly. Operating at high temperature ($400^{\circ}C$ to $1,000^{\circ}C$), SOFC eliminates the need for noble catalyst and, thus, is more cost-effective and also the high temperature enables direct reforming of hydrocarbons in SOFC, resulting in more flexible fuel choices [7–12].

Furthermore, at high temperature waste heat can be effectively recovered for power generation by driving gas turbine to enhance the overall energy efficiency [13–16]. Thus the electrical energy is produced from heat generated during the fuel cell operation.

The conventional type of SOFC is oxide ion conducting SOFC (O-SOFC) of which the electrolyte is commonly made of an oxide ion conducting material. But the most efficient type of the SOFC is the proton conducting which has many advantages as compare to that of the oxide ion conducting SOFC.

The fundamental operational mechanisms of conventional O^{2-} conducting SOFC and advanced H^+ conducting SOFC are illustrated in Fig 2a, and 2b for easy comparison. In a conventional O-SOFC, hydrogen fuel is fed to the anode and oxidant air (mixture of oxygen and nitrogen) is supplied to the cathode, oxygen ion flows through the electrolyte, and steam is formed as a byproduct and transported out of the anode. As the molar hydrogen consumption rate is equal to the molar steam generation rate, the gas pressure within the anode is not changed. Thus the transport of hydrogen and steam in the anode is entirely by diffusion process. On the other hand, the consumption of oxygen in the cathode-electrolyte interface causes both gas pressure gradient and concentration gradient in the cathode. Thus, oxygen is transported in the cathode both by permeation and diffusion.
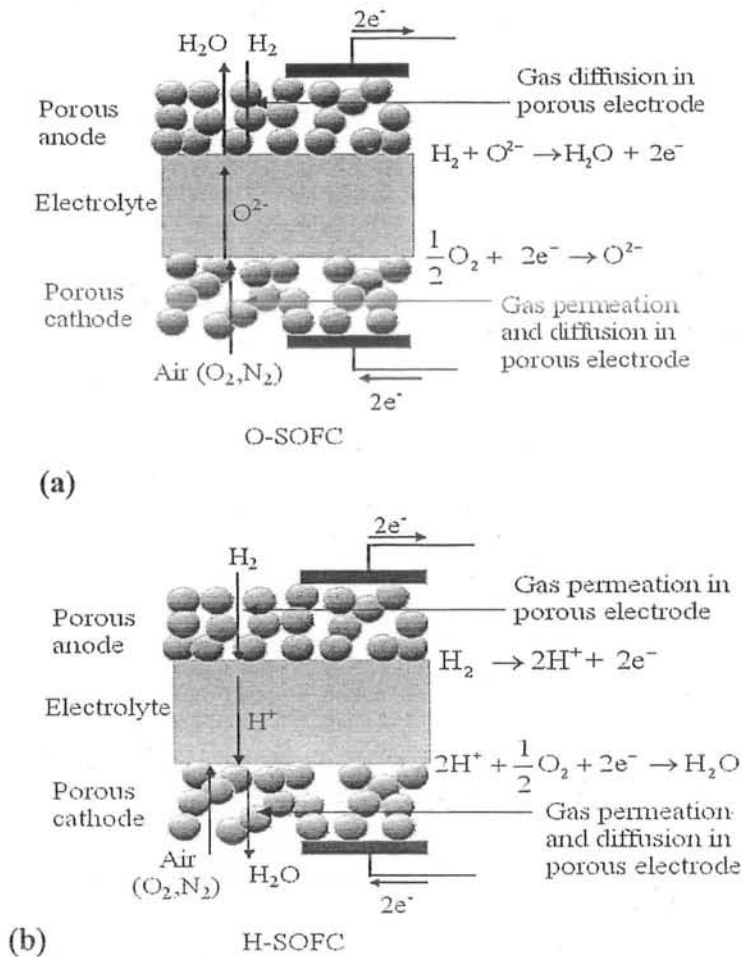
Figure 2: Operational mechanisms of (a) O^{2-} conducting SOFC and (b) H^+ conducting SOFC[10]

In H-SOFC, hydrogen is also fed to the anode. At the anode-electrolyte interface, H_2 is oxidized to H^+ and e^-. The electrons flow through an external circuit in the form of useful electricity, while the protons are transported through the proton-conducting electrolyte to the cathode. The consumption of hydrogen at the anode–electrolyte interface causes a pressure gradient in the anode. Thus, hydrogen will continue to flow to the cathode by permeation. At the cathode, O_2 is transported to the cathode–electrolyte interface and reacts with H^+ and e^- to form H_2O. The generated H_2O is then transported to the cathode surface and leaves the fuel cell. As the oxygen molar consumption rate is half of the steam molar generation rate, both the pressure gradient and gas concentration gradient are established in the porous cathode. Therefore, gas transport in the cathode is by diffusion and permeation. As the pressure at the cathode–electrolyte interface is higher than that at the cathode surface, the pressure gradient exerts a negative effect on the transport of O_2 from the cathode surface to the cathode–electrolyte interface.

3. Proton conduction mechanisms.

Proton is highly polarizing species due to its high charge density. It can strongly polarize the environment which leads to high binding energies. Speaking in terms of transport, this corresponds to a high degree of self-localization and implies a strong coupling of long-range proton motion to the dynamics of the proton environment. This is actually one common feature of all proton conduction mechanisms in quite diverse families of compounds [18].

Mostly it moves through the solutions as a part of the protonated species H_3O^+ by using the water molecules as vehicle [19, 20]. In1960s proton conduction in ice was explained by the Fischer et al, as a proton-phonon coupling [21]. These considerations were supported by the Marcus theory [22] which describes the mechanism of proton transfer in solutions and the theory of hydrogen tunneling trough metals [23]. All these mechanisms have one thing common that the mobile species (proton, electron, hydrogen) follow a moving structural pattern and it is the activation of this structural diffusion that controls the activation enthalpy of, e.g., proton diffusion.

In the case of proton mobility within hydrogen bonded liquids, this is usually the rearrangement of the hydrogen bond pattern, which requires thermally activated

hydrogen bond-breaking and bond-forming processes. This effect has particularly been studied for the mobility of excess protons in water. The main work on the conduction of proton trough the water was done by the Tuckerman et al, and Agmon [24, 25]. Essential features of the suggested mechanism are,

(i)   Intermolecular proton transfer occurs through rather short hydrogen bonds.

(ii)   This transfer is highly coupled to hydrogen bond-breaking and bond-forming processes.

(iii)   The position of the protonic charge follows the center of symmetry of the hydrogen bond pattern [26].

Although the proton conduction mechanism in hydrogen bonded networks comprises the interaction of many species., proton conduction mechanisms in oxides are usually less complex; this is because of the fact that protons are usually present at low concentrations as part of non interacting [27], positively charged point defects (generally hydroxide ions residing on oxide ion sites). These defects show significant hydrogen bond interaction with neighboring oxide ions, and it is the local dynamics of this hydrogen bonding that is the clue to the understanding of proton conduction mechanisms in perovskite-type oxides. Only in very few perovskite-type oxides, such as $Ba_2YSn_{O5.5}$ [28], very high proton content may add some complexity to the proton conduction mechanism.

3.1 Proton defects

The proton conduction is based on the existence of a proton defects in the ceramic electrolyte membranes which are created when the ceramic electrolyte membranes, containing oxygen vacancies which are shown by the square in the following equation, dissociates and absorbs water from a surrounding wet atmosphere.
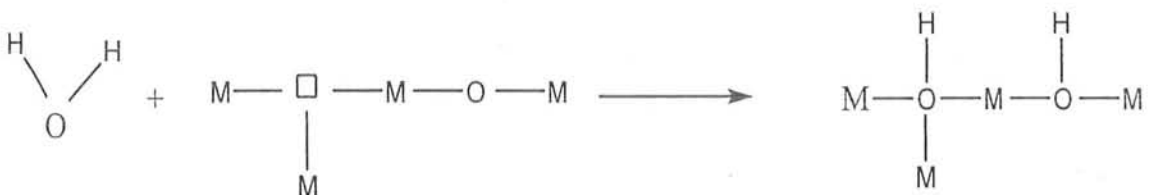
The process can be described well by the following equation:

$$O_O^X + V_O^{\bullet\bullet} + H_2O \longleftrightarrow 2(OH)_O^{\bullet}$$
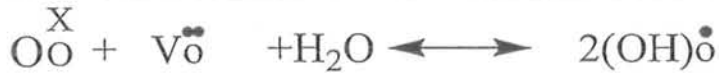
These proton defects are responsible for migration of the protons from one oxygen atom to the next involving neighboring proton defects as explained in the Fig. 3 from Iwahara [18] and kreuer [19].

A proton conducting solid oxide fuel cell with an aliovalent electrolyte like $BaCe_{0.8}Y_{0.2}O_3$, $SrZr_{0.8}Y_{0.2}O_3$, contains the oxygen vacancies as shown in the above equation which are produced to compensate an acceptor dopant. For the operation of such type of proton conducting solid oxide fuel cells initially the sufficient wet atmosphere is necessary to allow the formation of proton defects in the electrolyte.

Protons can show very strong binding interaction with that of the oxygen atoms which are the most electronegative species in the perovskite materials and form hydroxide ions. Therefore the position of protons within the perovskite type oxides is controlled by the oxygen atoms of the perovskites. Oxygen atoms provide some electron density to the protons so that they attain the H 1s character. The orientation of the hydroxide ion is then mainly determined by the hydrogen bonding with other, neighboring oxide ions, which is an attractive interaction, and interaction with the cations of the structure which of course is repulsive. Within the simple cubic perovskite structure i.e. a framework of corner-sharing undistorted oxygen octahedra, each oxygen has eight nearest oxygen neighbors with separations corresponding to the edge length of the octahedra, and four next nearest neighbors, which reside on the vertices of the four neighboring octahedra in the same plane.

Quasi-elastic neutron scattering experiments of some perovskite materials show that a proton can jump a width of 170pm and this length is interpreted as the separation between proton sites on the edges of neighboring octahedra corresponding to linear hydrogen bonding of the hydroxide ion to their nearest oxygen atom[29].

Molecular dynamics simulations of proton in some perovskites also show the similar results [30, 31]. Quantum molecular dynamic study of the $BaCeO_3$ [7] at 900K show the traces of proton confined to a donut with the hydroxide oxygen at the centre. This donut contains the proton sites. Thus by the use of proton probability density function of different perovskite materials proton sites have been found [32, 33].

However the position of proton is not certain and exact and the uncertainty of proton sites is actually reflecting the locally flat, free energy surfaces, especially in the perovskites with small lattice constants.

In perovskites with small lattice constants such as $SrTiO_3$ and $CaTiO_3$, the proton sites are closer to the plane formed by the hydroxide ion and its four next nearest oxygen neighbors, but for large lattice constants the only hydrogen bond interaction is within octahedra, while for small lattice constants, also hydrogen bonding to oxygen of neighboring octahedra appears to be possible. Hydrogen bonding is actually indicated by a small contraction (a few pm) of the average separation between the hydroxide ion and its eight nearest and four next nearest oxygen neighbors [34].

It is most likely the repulsion with the highly charged B-site cation and the attraction from the next nearest oxygen that a proton feels a push to move out of the octahedron edge. The resulting degree of hydrogen bond bending surely has severe implications on the proton conduction mechanisms

Once the proton defects are produced in the electrolyte the hydrogen gas is provided at the anode and oxygen at the cathode. Following reactions occur at the anode and cathode respectively

3.2 Anodic reaction

At the anode side hydrogen absorbs and get oxidize to convert into the protons and electrons. Hydrogen oxidation produces protons able to migrate on proton defects. Electrons flow to the outside circuit which is the origin of electricity in the solid oxide fuel cell as shown in the following equation.

$$H\!\!-\!\!H \ + 2O_O^X \ \longrightarrow \ 2OH_O^{\bullet} \ + 2\bar{e}$$

3.3 Cathodic reaction

At cathode, oxygen gas is supplied which absorb on the surface of cathode, take up electrons and get reduce to form the O^{2-} ions. These negative ions combine with the protons at cathode electrolyte interface and produce water and heat because this reaction is highly exothermic. This is the origin of heat produced from the fuel cell. Whole reaction at the cathode can be represented by the following equation.

$$1/2O_2 \quad + \quad 2e^- \quad + \quad 2OH_o^\cdot \longrightarrow H_2O \quad + \quad 2O_o^x \quad + HEAT$$

Water is the product of the cell reaction which accumulates at the cathode. Therefore atmosphere near the cathode remains wet. These water drops are evaporated by the air threshes from the surface of cathode.

4. Proton transport trough the electrolyte

The prorton conduction mechanicm can be explained by a very simple method as shown in Fig. 3.
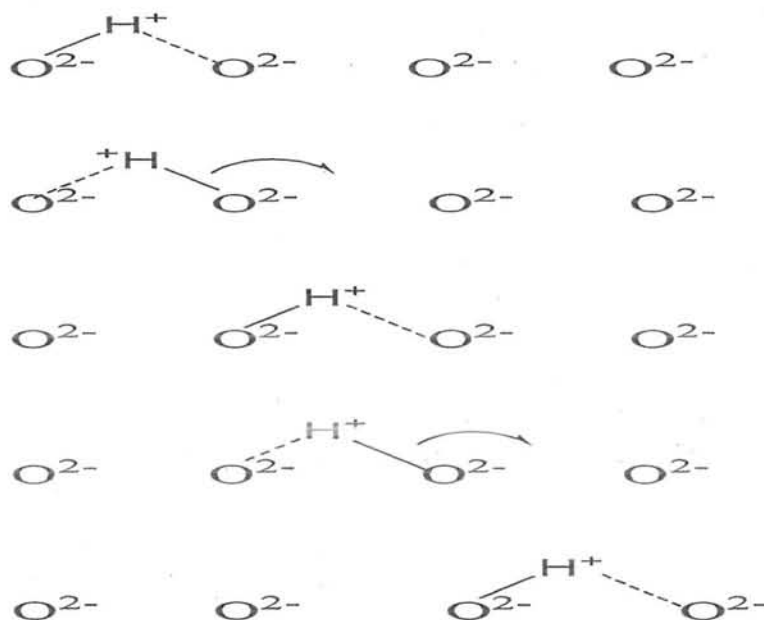
Figure 3: Mechanism of proton conduction through oxide ceramic electrolyte membrane [37-38].

By using the modern techniques like molecular dynamic simulation, Quasi-elastic neutron scattering, and μ-SR [35, 36] experiments the path and mechanism of proton transport in perovskites is determined. These techniques show that proton moves across the electrolyte by a series of jumps from one oxygen atom to the next as shown by the Fig. 3. This mechanism of movement of proton from one oxygen atom to the next nearest oxygen atom through jumping is called hoping mechanism and it can be well explained through the analogy with hoping movements of monkies from one tree to the next through branches of the trees. Flexibility of branches makes all these movements possible. Similarly the flexibility of hydrogen bonding i.e, making and breaking of the hydrogen bonds, makes the movements of the proton possible from one surface of the

10

electrolyte membrane to the other. This hoping of the proton from one oxygen atom to the next is called rotational diffusion. In this process proton form a covalent bond with one of the eighth oxygen atom. This covalent bond remains intact and proton moves around the oxygen atom and forms a donut keeping the oxygen atom at the centre. Thus the proton changes only the orientation. The energy required to change this orientation is provided by the hydrogen bond formation with the lattice oxygen which is an exothermic process. In this way proton first rotates around the oxygen atom and then move towards the next oxygen atom. This process is called rotational diffusion as shown by the Fig. 4. Formation and breaking of the hydrogen bonds and repulsion of proton from the positively charged metal atom play an important role in the rotational diffusion of the protons from one oxygen atom to the next one.
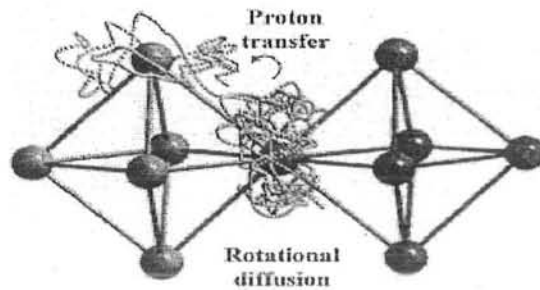
Figure 4: Demonstration of the interoctahedra rotational diffusion [39]

One proton links the two oxygen atoms as shown in the Fig. 3 and involves a slight contraction of the average OH/O separation and an expansion of the separation between the hydroxide ion and the two neighboring B-site cations as shown in Fig. 5 [40–41].
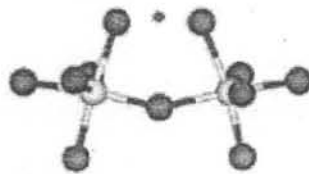
Figure 5: Demonstration of the O-H-O bond contraction and B-O-B bond expansion

Any proton conduction mechanism must at least partially compensate for these relaxation effects i.e. it must involve some host lattice adjustment in the transition state configuration.

Considering the large average oxygen separations (e.g., compared to hydrogen bonding in water) of typically 290–320 pm, this appears to be reasonable, but it seemed to be in

conflict with the strongly red-shifted OH-stretching absorptions in the IR spectra [42] indicating strong hydrogen bond interactions, which favor fast proton transfer reactions rather than fast reorientation processes, the latter requiring the breaking of such bonds. As the structural oxygen separation is larger than 290 pm in most perovskite type oxides and strong hydrogen bonds may only be formed for significantly lower separations, the free energy the system gains by hydrogen bond formation is competing with the free energy required for the lattice distortion involved in the OH/O contraction. Quantum-MD simulation of a protonic defect in cubic $BaCeO_3$ [43-44] demonstrates that these two free energy contributions are almost balanced for a wide range of oxygn separations (approximately 250–300 pm). In this way, short oxygen separations, which favor proton transfer, and large oxygen separations, which allow rapid bond breaking involved in rotational diffusion, correspond to similar free energies of the entire system and, therefore, have similar probabilities of occurring. Indeed, the simulation finds the protonic defect to form short but transient hydrogen bonds with all eight nearest oxygen neighbors. In the time-averaged picture seen in diffraction experiments, this leads only to a slight reduction of the structural OH/O separations but in most instant configurations one of the eight OH/O separations is reduced to about 280 pm as a result of hydrogen bonding [45]. Although the hydrogen bond interaction has a stabilizing effect of about 0.5 eV on this configuration [46], the bond is a soft high-energy hydrogen bond with extended bond length variations; this also leads to configurations where the protonic defect behaves almost like a free OH with small OH stretching amplitudes compare to the extended stretching vibrations in the hydrogen bonded state. From the thermodynamics of such ''dynamical hydrogen bonds' one may actually expect an activation enthalpy of long-range proton diffusion not more than 0.15 eV provided that the configuration O–H˙ ˙O is linear, for which the proton transfer barrier disappear at O/O separations less than about 250 pm. However, the mobility of protonic defects in cubic perovskite-type oxides has activation enthalpies of the order of 0.4–0.6 eV [47], which raises the question of which interactions are controlling the activation enthalpy of proton transfer? As already pointed out, in the average configuration the hydrogen bonds are bent to some extent.

There are certain factors which describe that how the energy required for the motion of proton trough the electrolyte is balanced with the energy released from hydrogen-oxygen bond formation.

1. Inspite of the strong hydrogen bonding the activation energy for rotational diffusion of protonic defects may be small.

2. The proton prefers an OH orientation away from the octahedral diagonal, probably because of the strong H $-Ce^{4+}$ repulsion. Thus the transient hydrogen bonds are not linear and additional energy is required to bring the hydrogen bonded complex close to linear, which favors proton transfer. This is brought about by an elongation of the B–O bonds [48], which explains the increase of the activation enthalpy under pressure.

3. Since the protonic defect may form transient hydrogen bonds with eight oxygen neighbors, thus OH orientation and OH–O separation have to non match in the transition state; there may be significant negative contributions to the proton diffusion entropy [49].

This change suppresses proton transfer for two reasons: there is a remaining proton transfer barrier even at low oxygen separations, and any proton transfer requires both energy and momentum transfer in this bent configuration. Experiments on the transient state configurations obtained from molecular dynamics simulations showed that the B–O bonds are elongated, which reduces the repulsion between the B-site cation and the proton and allows for the formation of an almost linear, short hydrogen bond in the transition state as shown in the Fig. 6.
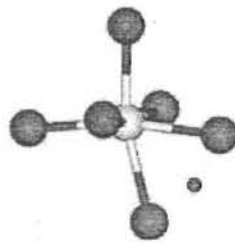
Figure 6: Linear hydrogen bond formation.

Although the H/B repulsion is reduced in this configuration, major contributions to the activation enthalpy arise from the B–O bond elongation and the proton transfer barrier. The importance of the H/B repulsion is also evidenced by the finding that the activation enthalpies of proton mobility in cubic perovskites with pentavalent B-site cations (I–V perovskites) are significantly higher than for perovskites with tetravalent B-site cations

13

(II–IV perovskites) [53]. On this background, proton mobility in III–III perovskite may be even higher, provided the oxide shows cubic symmetry.

The mechanisms just described provide a qualitative explanation that the highest proton conductivities are observed in oxides with the cubic perovskite structure [50]. All oxygen atoms in the cubic perovskites are equivalent and hence contribution of any extra activation energy for proton transfer is absent that may be generated by the non equivalence of the oxygen atoms as occur in the complex doped perovskites.

Also, deviations from the ideal cubic perovskite structure may bring about an increase of the activation enthalpy. This effect has been investigated in detail by comparing structural and dynamical features of protonic defects in Y(III) doped $BaCeO_3$ and Y(III) doped $SrCeO_3$ [51]. The large orthorhombic distortion of Y(III) doped $SrCeO_3$ has tremendous effects on the arrangement of the lattice oxygen. The cubic oxygen site degenerates into two sites with probabilities of 1/3 (O1) and 2/3 (O2). Owing to different chemical interactions with the cations, especially the strontium on the A-site, the oxygens on these sites show distinctly different electron densities (basicities) and, therefore, different binding energies for the proton. Whereas in $SrCeO_3$ the most basic oxygen is O1, in $BaCeO_3$ it is O2 as shown in the Fig. 7.
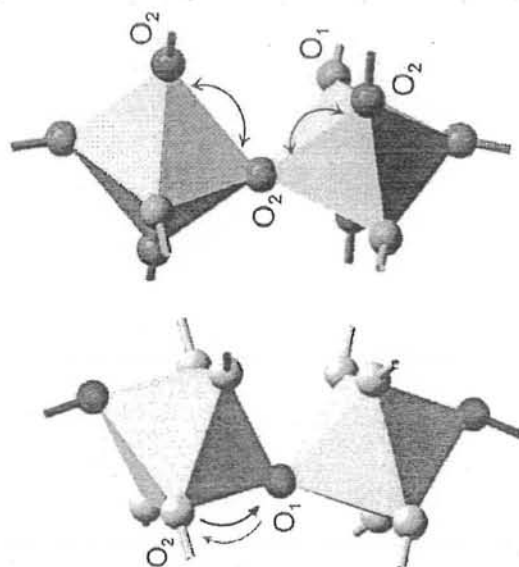
Figure 7: Effect of orthorhombic distortion of $BaCeO_3$ and $SrCeO_3$ on the basicity of oxygen [52].

Assuming that protons are associated with these sites most of the time, they may show long-range proton transport via the most frequent O2 sites in $BaCeO_3$, whereas long-

range proton transport in SrCeO$_3$ must involve transfer between chemically different O1 and O2 sites. The latter finding, together with the observed biasing of the rotational diffusion (defect reorientation), is thought to be the reason for the higher activation enthalpy and lower conductivity in SrCeO$_3$ compared with BaCeO$_3$.

5. Effect of temperature and water partial pressure on the proton conduction

The major impact of water vapor partial pressure in hydrogen fuel between 500 and 1000°C on the total and partial conductivities of the same electrolyte was described in detail by Dahl et.al [53]. At low temperature proton conductivity is found to dominate for almost all H$_2$O partial pressure where as oxygen ion conductivity is negligible except in very dry atmosphere. In contrast, at high temperature all types of conductivities become significant, oxygen ion conductivity having a large influence at almost all water partial pressure and proton conductivity contribution being almost negligible except at high water partial pressure. Thus at the anode side of a proton conducting SOFC, the lower the temperature the lower the influence of water partial pressure on proton conductivity; but in contrast, the higher the temperature the higher the need of a high water partial pressure to ensure predominant proton conductivity.

At the cathode side, the atmosphere is readily wet. But on this side also temperature has a major impact on proton conductivity. Iwahara [54, 55] did some experiments in wet air and showed that the higher the temperature between 500 and 1000°C, the lower the proton concentration and the lower the proton transport number, this number becoming lower than the oxygen ion transport number above 800 °C.

As a conclusion, a pure PCFC will require an operating temperature lower than 700 °C.

CHAPTER 2
EXPERIMENTAL

1. General Considerations

Most of the chemicals and reagents used such as $Ce(acac)_3$, $La(acac)_3$, $Ba(OAc)_2$, $Zr(acac)_4$, $Y(acac)_3$, $Y(OAc)_3$, $Sr(OAc)_2$, dmaeH, TFA, Sodium metal, THF, were purchased from Fluka, Merck, and Sigma Aldrich chemicals. Solvents were completely dried with sodium metal/benzophenone. All reactions were carried out under an atmosphere of dry argon using schlenk and glovebox techniques.

Sintering of all the samples was carried out at the temperature $T>1000°C$ using the Carbolyte-UK muffle furnace with controlled heating rate of $5°C/min$. The sintered material samples were crushed into fine powder using mortar and pistal.

Thermogravimeteric analysis of the perovskite ceramic membranes were carried out using METTLER TOLEDO TGA-851e with computer interface. The measurements were carried out under nitrogen and open air atmosphere using an alumina crucible at a heating rate of $10°C/min$.

Scanning electron microscopy (SEM) was carried out using a JEOL JSM -5910 scanning electron microscope with a beryllium window. Metallic elemental ratios were recorded on an EDX analyzer Inca-200 of Oxford instruments UK.

XRD peak patterns were collected using a PANalytical, X,Pert PRO diffractometer with Cu-Kα radiation.

FT-IR data were collected using the THERMO SCIENTIFIC (Nicolet 6700) FT-IR spectrophotometer. Only few peaks were appeared which were attributed to the presence of M-O bonds. The broad peaks were attributed to the O-H bonds.

The electrical conductivity measurements for all sample membranes were carried out using Keithley-2400 (USA) electrical conductivity meter between the temperature range of $30°C$ to $850°C$. Tube furnace (Carbolyte-UK) was used as a controlled heating source along with the temperature sensing multimeter (Uni-UT55).

2. General methods of synthesis of perovskite ceramic materials

There are several methods for the preparation of perovskite ceramic materials like solid state reaction method, sol-gel method, co-precipitation method, solution method etc.

Each method has its own advantages and disadvantages. All methods are briefly described below.

2.1 Solid State reaction Method

It is very simple method of the preparation of perovskite materials. In this method carbonates and oxides of required metals are mixed in stiochiometeric ratio. The whole mixture is ball milled for several hours to ensure complete mixing. By the ball milling 5% reaction is completed. Following the ball milling, reaction mixture is annealed at high temperature to complete the reaction in solid state. After annealing a single phase material is obtained. This can be proved through XRD analysis

Typical Example

Barium carbonate ($BaCO_3$), titanium oxide (TiO_2), and indium oxide (In_2O_3) are mixed in the suitable proportions. The powders are placed in a ball mill, mixed while grinding with acetone. After evaporation of the acetone, the mixture of powders is placed in a crucible and heated at a rate of $400\,^{o}C/h$ to a temperature of $1200\,^{o}C$, then kept at this temperature for 24 hours. The material is then cooled to room temperature at exactly the same rate at which it was heated, and then the product obtained is ground using a mortar and pestle so as to obtain a fine powder of the formula $Ba_{0.2}In_{1.6}Ti_{0.4}O_{4.4}(OH)_{1.6}$. It is a typical example of solid state reaction method.

2.2 Sol-gel method

This is the most commonly used traditional method in which nitrate salts of the reactants react in the presence of citric acid at certain pH. Citric acid act as the chelating agent and polymerize the reactants to convert them into product. Following polymerization a gel like product is obtained which is burnt at high temperature to obtain the powder of the material. It is crushed and again annealed at much higher temperature at which the solid state reaction occur and inphase material is produced.

Typical Example

The typical example of this process is the preparation of Co-doped ceria electrolytes. $Ce_{0.8}La_{0.2}Y_1O_3$ was synthesized by the sol–gel method using cerium nitrate, yttria, and lanthana as starting materials. Cerium nitrate was dissolved in deionized water and the desired amounts of yttria and lanthana were dissolved in nitrate solution. They were mixed together with citric acid solution. The pH value of the mixed solution was

adjusted with ammonia solution under continuous stirring at 70°C and homogeneous sol was formed. With the evaporation of water, a yellow sponge-like gel was obtained, The gel was placed in a 80°C drying oven, where the gel occurred self-igniting reaction and became light yellow powder, which was ground and calcined at 800°C in air for 2 h. The dried powders were ground in an a mortar and then pressed to obtained cylindrical pellets. The pellets sintered at 1500°C in air for 9 hours. [56]

2.3 Co-precipitation method

In this method some precipitating agent such as $(NH_4)_2CO_3$ is used to obtain the product. The precipitates obtained then filtered and air dried. The dried powder then calcined at much higher temperature normally more than 1000K to obtain a single phase perovskite material.

Typical Example

The typical example of co-precipitation method is the preparation of Yttrium doped strontium zirconates. In this method, a stoichiometric mixture of the same metal nitrate solutions and $(NH_4)_2CO_3$ solution were prepared. The metal nitrate solution is added dropwise to the $(NH_4)_2CO_3$ solution. Carbonate anions are required in order to precipitate strontium as $SrCO_3$ because $Sr(OH)_2$ is soluble in water at all pH values. The resulting precipitate consisted of Zr and Y hydroxides and Sr carbonates. It is filtered using a Buckner funnel and dried overnight in air at 400 K. The powder is then treated in air at 1.0 K/s to 1373 K for 4 h in order to form the perovskite phase. [57]

2.4 Solution Method

It is very simple method used to prepare the perovskite materials. In this method reactants used are the metal β-diketonates and metal acetates in some organic solvent such as toluene or tetrahydrofuran (THF). These metal complexes react together to give a clear solution in the presence of some bridging ligand such as aminoalcohols and triflouroacetic acid. Solvent is evaporated by the vacuum evaporation and a powder material is obtained. This powder is sintered at the high temperature to obtain a single phase perovskite material. The preference of solution method over the other methods is due to the following facts.

18

2.4.1 Advantages of the solution method

Metal organic precursors react in the organic solvent to give the clear solution which can be concentrated to crystallize the material i.e, crystallization is easier by this method then any other method. Annealing is done at relatively lower temperature while much higher temperature is required for other methods. Reaction is preceded in vacuum and argon atmosphere which removes the possibility of any impurity from the solvent or air. Thin films can be deposited from the clear solution by CVD. Solution method is a relatively quicker method for the preparation of perovskite materials.

3. Instrumental techniques of Characterization

3.1 X-ray Diffraction:

X-ray diffraction is a tool for the investigation of the fine structure of matter. Powder x-ray diffraction technique is helpful in determining the crystalline nature and phase purity of the mixed metal oxides. The diffraction pattern generated allows to determine the chemical compound or the phase composition of the mixed metal oxides and the crystallite size with the help of the Deby Scherrer,s equation.

X-ray diffraction is mostly used as a finger print method for detecting the presence of a known compound or phase in a product. A huge library of powder patterns of known compounds is present as ICDD (International Centre for Diffraction Data) files. When the diffraction pattern of the powder sample has been measured and both the d_{hkl} values and d-spacing and intensity of the lines recorded, these can be matched against the patterns of known compounds in files.

The qualitative analysis and purity check of the sample is possible but does has the limitations for the amorphous samples or if the impurity increases more than 5%.

Powder diffraction can be used for differentiating mixture of small crystals, determining phase diagrams and deciding whether different metal containing structure are isomorphs.

3.2 Scanning Electron Microscopy (SEM)

It is a surface imaging technique based upon the utilization of secondary electron beam. SEM provides higher magnification with greater depth resolution than other magnifying microscopes. High energy electron beams are focused to the small area on the surface of

the material which interact with the electrons of the material atoms and as a result of this interaction, elastic and inelastic reflections of the incident electrons takes place. The electrons which are reflected by the elastic collisions are called back scattered electrons (BSE). Inelastic collisions of the incident electrons generate the secondary electrons from the inner shells of material atoms due to which x-rays are produced. Different detectors are used to record the all signals. X-rays produced are used for the elemental analysis and electron beams are used to magnify the image of the material surface by the principle of electron microscope.

SEM images may become distorted by the surface potential builds up on insulators and in order to overcome this ambiguity the insulator surface is coated with thin conducting layer to dissipate the surface charge. SEM produce high magnification, i.e, more than 500,000 times the original size.

One of the most common analytical attachments to the SEM is the energy dispersive x-ray spectrometer (EDX). The useful energy range for EDX system is from 1.0 to 220keV. The analysis depth is dependent on the path length of the x-rays and not the primary electron beam. As a result, EDX signals may originate from depth of 0.5μm or more.

Due to pulse counting mode of EDX system, it has ability to detect the characteristic x-rays for all elements. Therefore, EDX system takes much shorter time to scan the complete spectrum. The detector used with EDX is of Li-doped Si that requires liquid nitrogen cooling to keep the Li from diffusing and rapidly degrading the detector's performance.

3.3 Thermogravimetric Analysis

Thermal Gravimetric analysis (TGA) is a destructive analytical technique that measures the weight change (gain or loss) of a material as a function of temperature and is used to measure the thermal stability and fraction of volatile components of the material. As materials are heated, they loose weight from a simple process of drying or from complicated chemical reactions that liberate gases. The gain in weight in the material is due to the reaction with the atmosphere in the testing environment. The measurement is normally carried out in air or in an atmosphere of nitrogen, helium or argon.

The presence of oxygen vacant sites in the perovskite ceramic materials are assessed by heating the material in the oxygen atmosphere and then in nitrogen atmosphere at high temperature and recording its weight. Gain in weight in case of oxygen atmosphere and no change in weight in nitrogen atmosphere proves that material is oxygen deficient and reacts with the atmospheric oxygen at high temperature to fill the oxygen vacant sites.

3.4 FT-IR Spectroscopy

FT-IR spectroscopy is used as an auxiliary technique for the identification of M-O (metal-oxygen bond) bonds present in the perovskite ceramic materials. Impurities present in the materials can also be investigated by this technique. This technique is also helpful in determining the O-H moiety present in the ceramic membranes as proton defects. FT-IR provides valuable information regarding the different functional groups present in the materials but it is not reliable in structural analysis of heterometallic materials because of the problem of masking of important bands. Some times the spectrum becomes so complicated that it becomes difficult to resolve the characteristic absorption bands.

4. Experimental Synthesis

4.1 Synthesis of $La_{1.0}Y_{0.2}Ce_{0.8}O_{3-\delta}$ (1)

0.5mL of N, N-dimethylaminoethanol was added into the mixture of 3.137g (5mmol) of La(acac)$_3$ gel in 20mL tetrahydrofuran (THF) in Schlenk tube. Transferred into it the 2.65g (4mmol) of Ce(acac)$_3$ and 0.386g (1mmol) of Y(acac)$_3$. Dark red, clear solution was stirred for 4h and evaporated to dryness. Reddish powder obtained was sintered at 1000°C. Resulting powder which was expected to be $La_{1.0}Y_{0.2}Ce_{0.8}O_{3-\delta}$ characterized by XRPD and found to be in single phase. FT-IR/cm^{-1}: 416(s), 403(s).

4.2 Preparation of $Ba_{1.0}Y_{0.2}Ce_{0.8}O_{3-\delta}$ (2)

0.255g (1.0mmol) of Ba(acetate)$_2$ was transferred into the mixture of 0.349g (0.8mmol) of Ce(acac)$_3$ in 15mL of N-N dimethylaminoethanol in a Schlenk tube under inert atmosphere and constant stirring. In a separate flask a mixture of 0.78g (0.2mmol) of Y(acac)$_3$ in 3mL of trifloroacetic acid (TFA) was prepared and transferred to the schlenk tube through canola. Clear yellow solution was stirred for 4h and evaporated to

dryness. The fluffy powder obtained was sintered at 1100°C. Resulting ceramic material of green color was characterized by XRPD and found to be in single phase. FT-IR/ cm⁻¹: 430.0(s), 403.2(s)

4.3 Synthesis of $Sr_{1.0}Y_{0.2}Zr_{0.8}O_{3-\delta}$ (3)

0.5mL of triflouroacetic acid (TFA) was added into the suspension of 0.205g (1mmol) Sr(acetate)₂ in 20mL tetrahydrofuran (THF) in Schlenk tube. In a separate flask a solution of 0.390g (0.8mmol) of Zr(acac)₄ and 0.78g (0.2mmol) of Y(acac)₃ in THF was prepared by the addition of 0.5mL of N,N-dimethylaminoethanol and transferred to the schlenk tube trough canola. Clear mixture was stirred for 6h and evaporated to dryness. Yellowish green powder was sintered at 1000°C. The resultant ceramic powder which was expected to be $Sr_{1.0}Y_{0.2}Zr_{0.8}O_{3-\delta}$ characterized by XRPD and found to be in single phase. FT-IR/ cm⁻¹: 523.6(s)

CHAPTER 3
RESULTS AND DISCUSSION

Mixed-metal oxide materials can be prepared easily by using the organic metal precursors such as metal β-diketonates, acetates, and alkoxides.The reactions can occur under mild conditions using non polar solvents in the presence of some chelating ligands such as trifloroacetic acid (TFA) and N-N dimethylaminoethanol (dmaeH) . These chelating ligands improve the solubility of the reacting precursors in the non polar solvents. Here we obtain the clear solution of the metal precursors by using these chelating ligands. The clear solution is evaporated to dryness to obtain the dry powder. This powder contains metals and organic ligands. Sintering the powder at high temperature in air evaporates the organic ligands and mixed metal oxide materials are obtained as a final product.

1. Characterization of $La_{1.0}Y_{0.2}Ce_{0.8}O_{3-\delta}$ (1)

1.1 X-Ray diffraction pattern
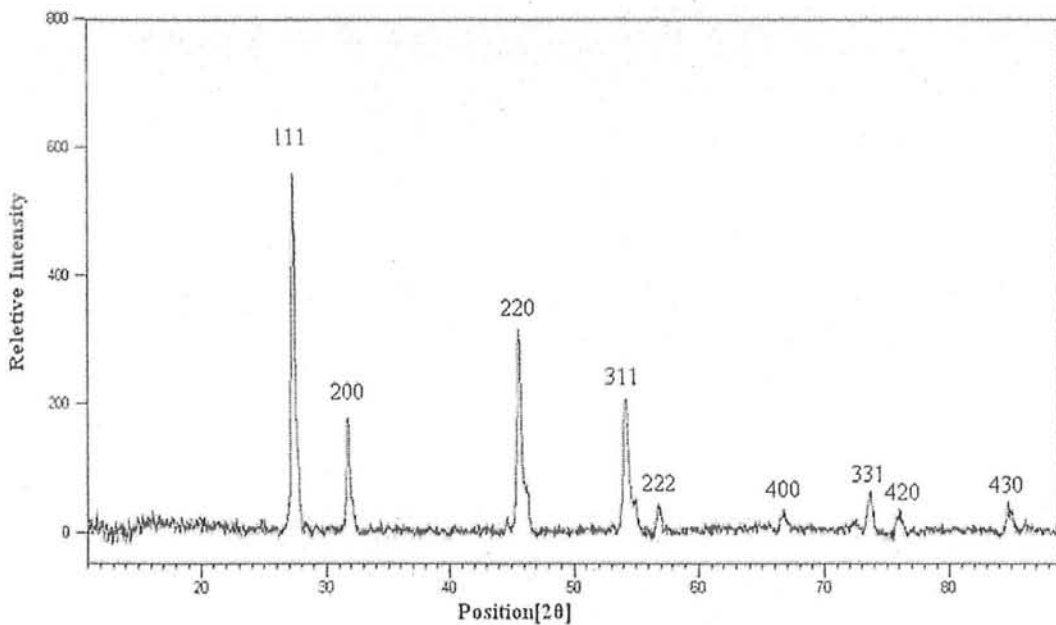
Figure 8: X-ray diffraction pattern of $La_{1.0}Y_{0.2}Ce_{0.8}O_{3-\delta}$ obtained at 1000°C.

The crystal structure of the decomposed oxide ceramic powder was determined by X-ray diffraction (XRD) analysis using a PANalytical X-ray diffractometer (monochromated Cu Kα radiation, λ=0.15418nm; operated at 40KV) at room

23

temperature in the Bragg angle range of $10°$ to $90°$. The particle size, of the ceramic powder was estimated using the scherrer's formula given below.

$$D = \frac{0.94\lambda}{\beta_{1/2} \; Cos\,\theta}$$

Where $\beta 1/2$ is the 2θ value of peak position at full width at half maximum (FWHM), λ is the wavelength of the Cu Kα X-ray and θ is the value of peak position. The particle size calculated by the Scherrer,s formula is 17nm.

XRD spectrum of the decomposed ceramic powder confirmed that the sample is single phase with cubic structure. All peaks can be indexed to miller indices (111), (200), (220), (311),(222),(400), (331), (420), and (430), respectively. The peak pattern of the $La_{1.0}Y_{0.2}Ce_{0.8}O_{3-\delta}$ show a good matches with the standard values [58]

1.2 Energy Dispersive x-ray (EDX) analysis of $La_{1.0}Y_{0.2}Ce_{0.8}O_{3-\delta}$
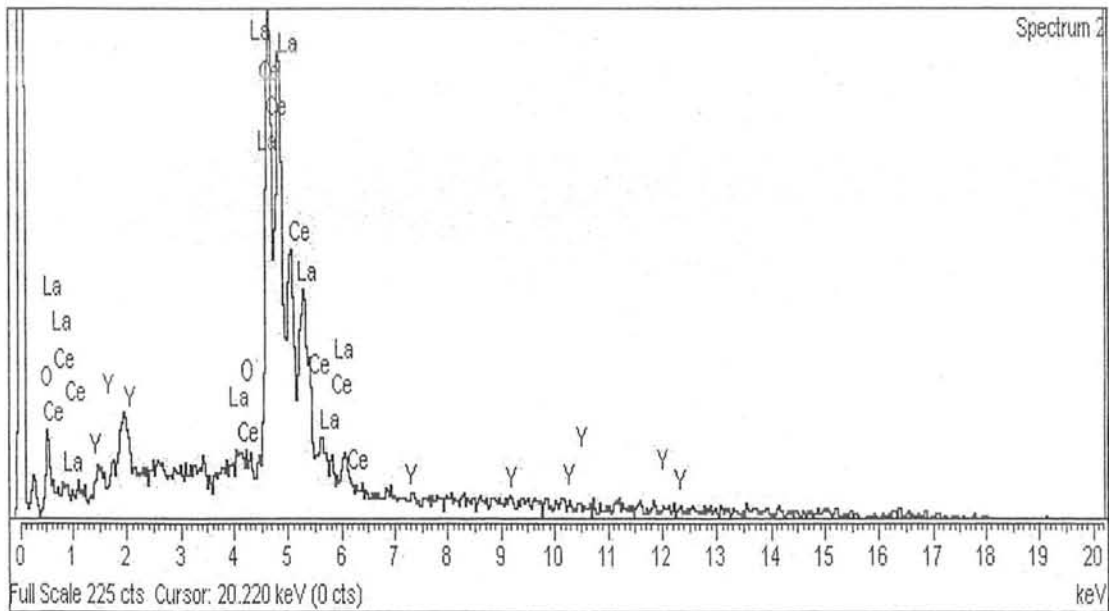
Figure 9: EDX spectrum of the $La_{1.0}Y_{0.2}Ce_{0.8}O_{3-\delta}$

EDX is an analytical technique which is used to determine the chemical composition of the material. High energy electron beam is focused on the surface of the material which interacts with the inner shell electrons of the material atoms and knocks them out by

strong collisions. So the electron vacancies are generated in the inner shells. Electrons from the outer shells jump into the electron vacancies in the inner shells. When electrons jump from outer shell into the inner shells, the energy is released in the form of x-rays. These x-rays are the finger print for each element present in the material because each element has its own fixed quantum energy levels. The energy of the x-rays is equal to the energy difference between the two quantum levels of the atom. Due to the pulse counting mode of the EDX system it has the ability to detect the x-rays of all elements. Therefore it is a most reliable technique for determination of proportion of the different elements present in the material sample. The distribution of the different elements in the $La_{1.0}Y_{0.2}Ce_{0.8}O_{3-\delta}$ is illustrated in the EDX spectrum in the Fig. 9. The relative abundance of each element is given in the Table 2.

Table 2: Elemental ratio of the $La_{1.0}Y_{0.2}Ce_{0.8}O_{3-\delta}$

Elements	Elemental Ratio (W%)	Molar Ratio
La	43.75	0.95
Ce	37.0	0.792
Y	4.8	0.16
O	14.45	2.70

The elemental ratio which is determined from the EDX analysis is in good agreement with the stoichiometeric values of the different elements used for the reaction. Hence the results of XRD and EDX shows that the material is single phase crystalline powder with the elemental ratio same as that was mixed.

Molar ratio of oxygen is slightly less than the required which indicates that the oxygen is deficient in the structure of the electrolyte membrane. Oxygen deficiency is important characteristic for the electrolyte ceramic membranes.

The scanning electron micrograph of the $La_{1.0}Y_{0.2}Ce_{0.8}O_{3-\delta}$ is not very clear, however by zooming the SEM micrograph, the morphology of the material surface become much clear. The material has uniform particle distribution with non clear grain boundaries of the particles and coarse surface morphology.
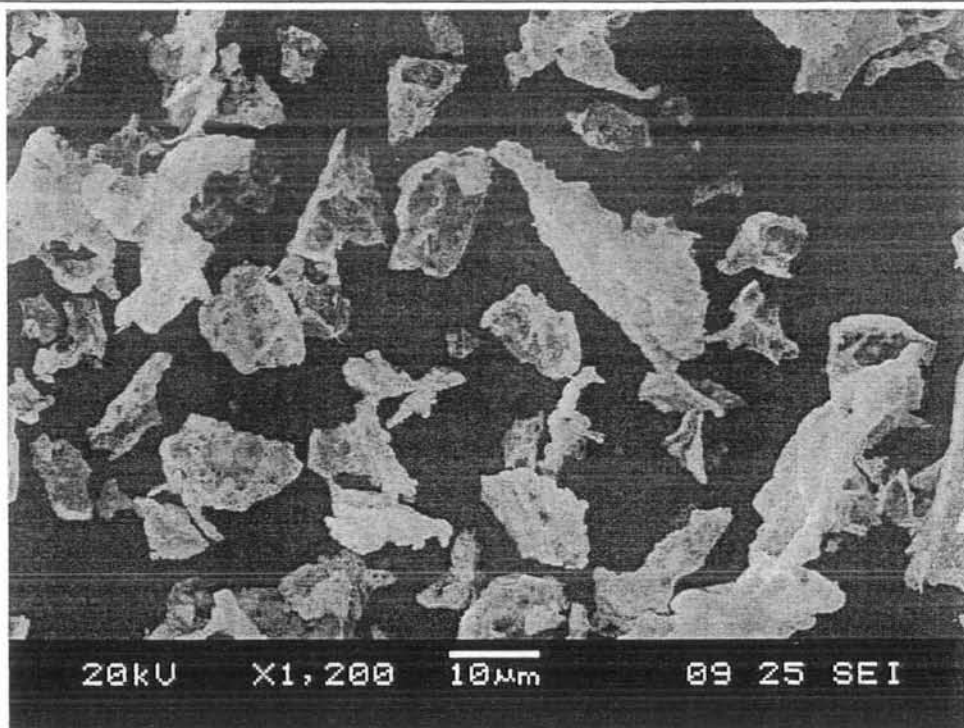
Figure 10: SEM micrograph of the $La_{1.0}Y_{0.2}Ce_{0.8}O_{3-\delta}$

1.3 Thermogravimetric analysis (TGA) of $La_{1.0}Y_{0.2}Ce_{0.8}O_{3-\delta}$

TGA is performed in open air and inert atmosphere using the instrument METTLER TOLEDO (TGA-851e). Thermogram of the $La_{1.0}Y_{0.2}Ce_{0.8}O_{3-\delta}$ shows a small gain in weight with increase in temperature, from room temperature to $150^{\circ}C$ and then start to lose weight with increase in temperature up to $300^{\circ}C$. Beyond $300^{\circ}C$ the material start to gain weight continuously up to $1100^{\circ}C$.

1.3.1 Thermogarvimeteric analysis of $La_{1.0}Y_{0.2}Ce_{0.8}O_{3-\delta}$ in O_2 atmosphere.

The gain in weight shows that $La_{1.0}Y_{0.2}Ce_{0.8}O_{3-\delta}$ react with the atmospheric oxygen at high temperature and let it to reside in the vacant sites present in the surface as well as in the bulk of the electrolyte material.

The presence of oxygen vacant sites in the proton conducting electrolyte membranes is important because of the fact that formation of proton defects in the electrolyte membrane depends upon the presence of oxygen vacant sites and proton conductivity depends upon the presence of proton defects. These oxygen vacant sites in the electrolyte material are filled by the water vapors when expose to the humid air. Electrolyte material split the water molecules into hydroxide ion and protons.

26

Hydroxide ions fill the oxygen vacancies and protons attach to the lattice oxygen. Thus two proton defects are produced by splitting a single water molecule. The weight loss upto 300°C might be due to the loss of these of proton defects which are not maintained at high temperature without the continuous supply of wet hydrogen. Beyond 300°C the weight increment is rather large. This is because of the fact that oxygen in the atmosphere fills the oxygen vacant sites along with the generation of the electron holes. These oxide ions and electron holes take part in conductivity of the electrolyte material in dry atmosphere i.e, when wet hydrogen is not available. The weight gain by the electrolyte membrane at high temperature and under oxygen atmosphere is clear indication of the fact that the electrolyte material react with the atmospheric oxygen at high temperature and vacant sites are filled by the oxygen along with the generation of electron holes. Thus thermogravimeteric analysis provides important informations regarding the characterization of the electrolyte membranes.
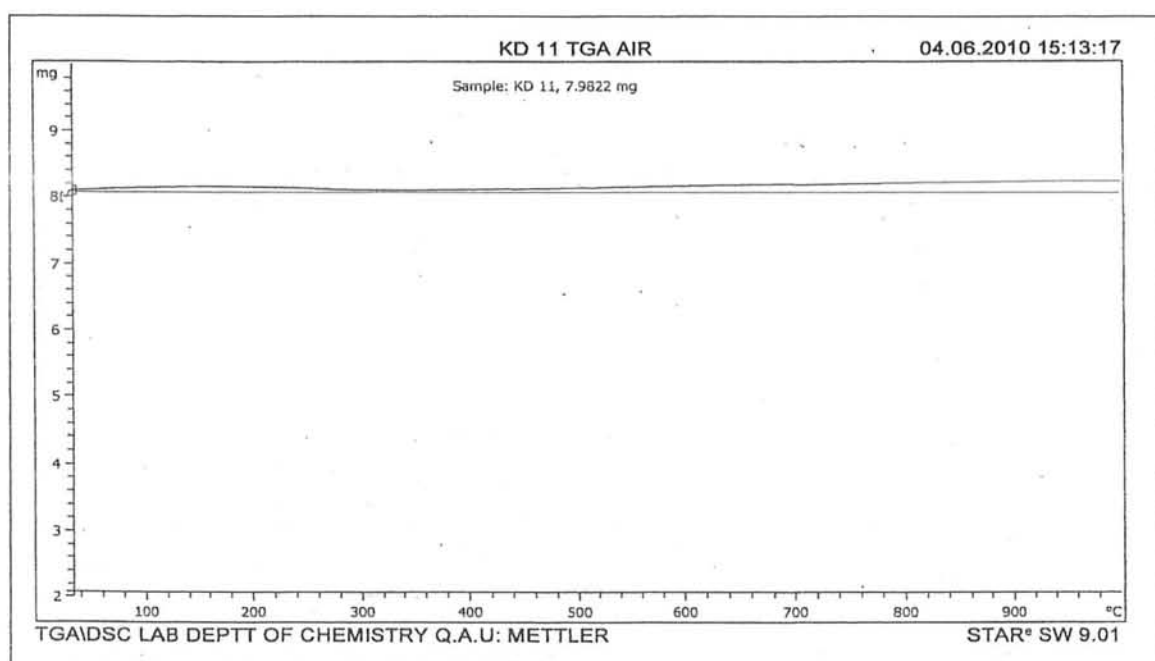
Figure 11: Thermogram of the $La_{1.0}Y_{0.2}Ce_{0.8}O_{3-\delta}$ in air.

The percentage weight gain by the electrolyte material is shown in the Table 3. The percent weight gain is small which shows that the concentration of oxygen vacant sites is not too high.

Table 3: Weight gain by the $La_{1.0}Y_{0.2}Ce_{0.8}O_{3-\delta}$ at $1000^{\circ}C$ in O_2 atmosphere

Initial weight	Final Weight	Weight Increment (%)
7.98mg	8.28mg	3.75

Further confirmation of the presence of electron holes and oxide ions is provided by the electrical conductivity measurement. Oxygen deficient electrolyte material shows the electrical conductivity in the open atmosphere and at high temperature due to the presence of electron holes and oxide ions i.e, p-type conduction.

$$V_O^{\bullet\bullet} \;+\; 1/2O_2 \;\rightleftharpoons\; O_O^X \;+\; 2h^{\bullet}$$

1.3.2 Thermogravimeteric analysis of $La_{1.0}Y_{0.2}Ce_{0.8}O_{3-\delta}$ in N_2 atmosphere.

Under inert conditions such as nitrogen atmosphere the weight change of the electrolyte material $La_{1.0}Y_{0.2}Ce_{0.8}O_{3-\delta}$ as a function of temperature is almost zero as shown in the Fig.12. It means that electrolyte material $(La_{1.0}Y_{0.2}Ce_{0.8}O_{3-\delta})$ do not react with the nitrogen even at high temperature. Thermal analysis of the $La_{1.0}Y_{0.2}Ce_{0.8}O_{3-\delta}$ under oxygen atmosphere and inert atmosphere provide the information about the oxygen deficient nature of the electrolyte membrane.
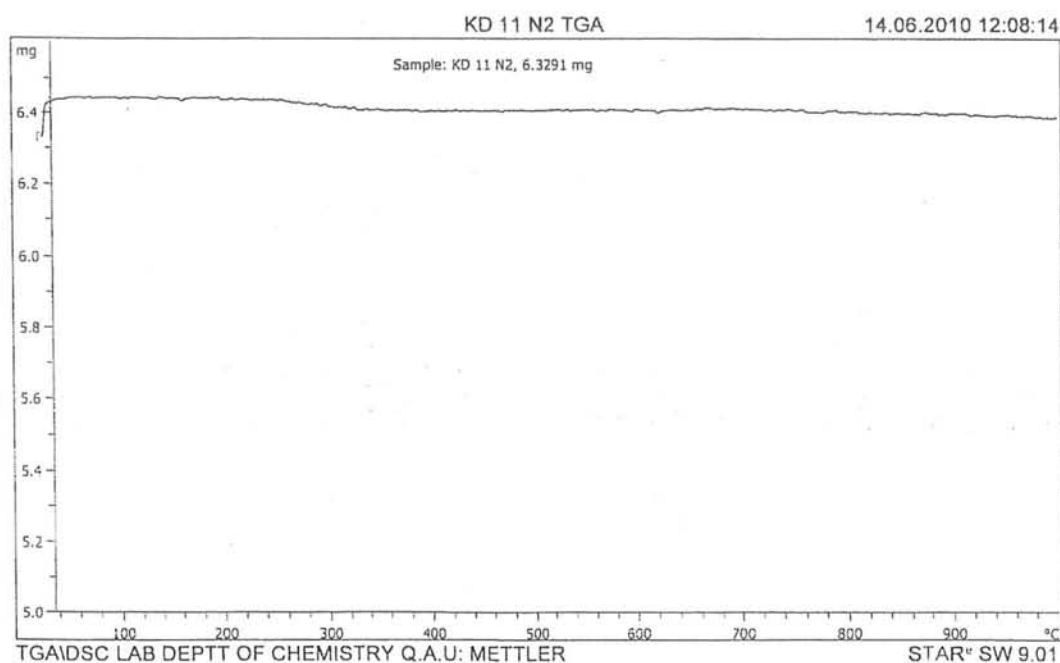
Figure 12: Thermogram of the $La_{1.0}Y_{0.2}Ce_{0.8}O_{3-\delta}$ in nitrogen atmosphere.

1.4 Electrical conductivity of $La_{1.0}Y_{0.2}Ce_{0.8}O_{3-\delta}$ electrolyte membrane

In order to measure the electrical conductivity of the $La_{1.0}Y_{0.2}Ce_{0.8}O_{3-\delta}$, the powder was pressed in the form a membrane. For this purpose dye press method was used. Powder material was poured into the dye and pressed under high pressure using the hydraulic press. Circular membrane having diameter 13mm and thickness 1.15mm was prepared. This membrane was kept between the electrodes of the electrical conductivity meter (Keithley, 2400) and the whole assembly was kept in the tube furnace along with the temperature sensing probe of the multimeter (UNI, UT55) to monitor the effect of temperature on the conductivity. The conductivity of the $La_{1.0}Y_{0.2}Ce_{0.8}O_{3-\delta}$ as a function of temperature is shown in the Fig. 13 .
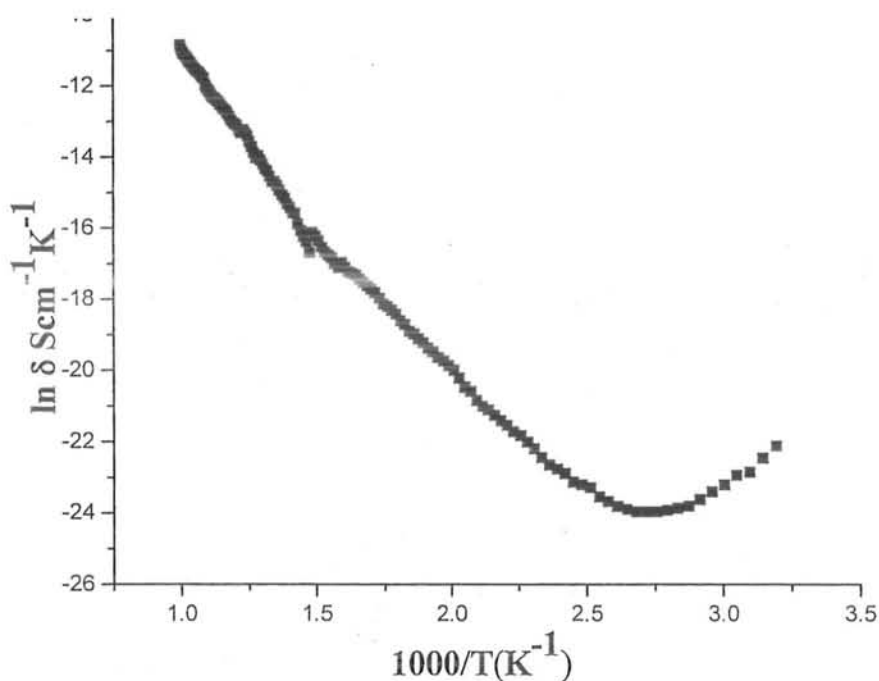
Figure 13. Arrhenius plot for electrical Conductivity of $La_{1.0}Y_{0.2}Ce_{0.8}O_{3-\delta}$ electrolyte.

The activation energy calculated from the arrhenius plot is Ea=0.76eV which is the minimum amount of energy required by the electrolyte membrane to show electron hole and oxide ion conductivity.

29

Above figure shows that conductivity of the electrolyte material increases with increase in temperature after certain transition temperature. At room temperature the material is resistive having very low conductivity.

It is required for the proton conducting ceramic electrolyte materials to be good ionic conductors and bad electron conductors. It is an important property of the ceramic material to use as an electrolyte in the solid oxide fuel cells. During the fuel cell operation, H_2 oxidized at the anode surface and convert into the protons and electrons. Protons pass trough the electrolyte membrane and reach from one side to the other i.e, from anode electrolyte interface to the cathode electrolyte interface and electrons move through the external circuit and reach the cathode material where they find the oxygen and reduce it into oxide ions. These oxide ions and protons react to produce water at the cathode electrolyte interface and water droplets are transferred to the cathode surface from where they are evaporated. Oxidation of the hydrogen occurs at the anode as follows.

$$H\text{---}H \longrightarrow 2H^+ + 2e^-$$

Electrons produced as a result of oxidation are moved towards the cathode through an external circuit wire and are origin of the electricity in the fuel cell. We draw the energy from these moving electrons to generate electricity. If electrons find path other than the external wire circuit then the efficiency of the fuel cell will decrease. Therefore in order to make fuel cell highly efficient the electrolyte material should be only ionic conductor and electronic insulator.

The electrical conductivity of the material $La_{1.0}Y_{0.2}Ce_{0.8}O_{3-\delta}$ is very small i.e, few micro amperes current is passed trough the electrolyte at 200V as shown in the Fig. 13, as this conductivity is determined in the dry atmosphere therefore it is not due to the protons but due to oxide ions and electron holes.

Ionic conductivity of the proton conducting electrolytes depends upon the presence of proton defects and the most important reaction leading to the formation of proton defects at moderate temperature is the dissociative absorption of water, which require the presence of oxide ion vacancies. The vacancies may be formed intrinsically by varying the ratio of the main constituents, or they may be formed extrinsically to

compensate for an acceptor dopant. In order to form the proton defects water from the gas phase dissociates into a hydroxide ion and a proton as shown below.

$$H_2O \longrightarrow OH^- + H^+$$

The hydroxide ion fills an oxide ion vacancy, and the proton forms a covalent bond with the lattice oxygen. Thus two positively charge protonic defects are formed. Such charge defects diffuse into the bulk of the electrolyte only when accompanied by the counter diffusion of oxide ion vacancies [59]. This implies that such electrolytes show some oxide ion conductivity in the dry state and have affinity for chemical diffusion of water. Oxygen deficient electrolyte ceramic materials absorb oxygen when encounter high oxygen partial pressure at high temperature. Oxygen fills the vacant sites and is accompanied with the generation of electron holes [60-62]. These holes are similar to the holes produced in the p-type silicon semiconductors. Thus we can deduce the results that the conductivity shown by the electrolyte at high temperature and under dry conditions is due the presence of electron holes and oxide ions. Hence we can say that at higher temperature the electrolyte material show the p-type conduction [63] just like that of the silicon semiconductors. Doping of cerium with yttrium causes two opposite effects. On the one hand it causes the random distribution of oxygen vacancies which lead to the decrease in activation energy of conduction and increase in ionic conductivity [64, 65].

On the other hand, the deviation of the lattice parameter from pure CeO_2 are enlarged which lead to the increase in activation energy of conduction and decrease in ionic conductivity. Hence we can make an appropriate electrolyte by using the appropriate doping concentration.

Oxide ion conducting materials show high ionic conductivity in the dry air because the oxide ion vacancies are filled by the oxygen of the air e.g., the cathode of the SOFC which is mixed ionic and electron conductor show very high conductivity in the dry atmosphere. But the proton conducting materials need water partial pressure to fill the oxide ion vacancies and for the formation of the proton defects. Open atmosphere contains a very small amount of water which is not sufficient to produce the proton defects in the electrolyte hence it shows very small conductivity in dry air.

Therefore the presence of proton defects in the proton conducting electrolyte materials is important property of these materials. These proton defects in the electrolyte material

31

can be traced by the FT-IR spectroscopy. It is clear from the FT-IR spectrum, recorded under dry conditions that O-H peak is absent which confirms the absence of proton defects. This result is a clear indication of the fact that open air atmosphere has not sufficient amount of water to produce the proton defects. Thus oxide ion and electron hole conductivities are dominant under dry atmospheric conditions.

Whenever water vapors are available to the proton conducting electrolyte membranes the proton defects are produced and proton conductivity prevails all other conductivities .In order to confirm the presence of proton defects in the electrolyte membrane under moist conditions the electrolyte membrane was exposed to the wet air i.e. air carrying sufficient amount of steam. After three hours the FT-IR spectrum was recorded. A broad peak appeared near $3321 cm^{-1}$ which was attributed to the presence of hydrogen bonded O-H-O stretch. Therefore during fuel cell operation the wet hydrogen is provided initially to form the proton defects.

Proton conductivity dominate the electron hole and oxide ion conductivity when a proton source is available i.e. hydrogen or wet air containing sufficient amount of water vapors.
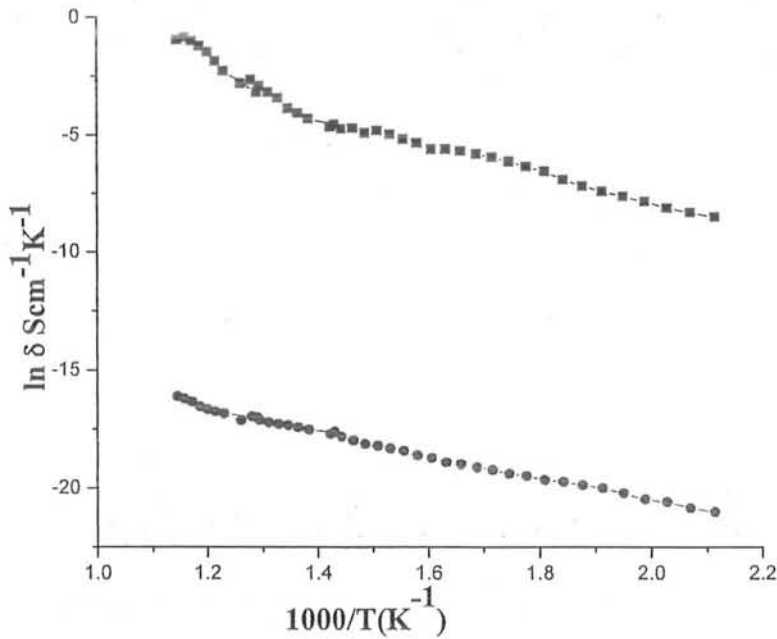
Figure 14: Comparison of the electrical conductivities of $La_{1.0}Y_{0.2}Ce_{0.8}O_{3-\delta}$ in dry air (I) and humid air (II) at T= 300-600°C

The difference in the ionic conductivities in dry and wet air is obvious from the Fig 14. The ionic conductivity of $La_{1.0}Y_{0.2}Ce_{0.8}O_{3-\delta}$ in wet air is much higher as compare to that in dry air. In the presence of wet air proton defects are produced in the electrolyte material. Protons are small ions and move faster as compare to oxide ions. Therefore whenever protons are available the conductivity of proton conducting ceramic electrolytes increases drastically.

1.5 FT-IR analysis of $La_{1.0}Y_{0.2}Ce_{0.8}O_{3-\delta}$

FT-IR spectrum of the $La_{1.0}Y_{0.2}Ce_{0.8}O_{3-\delta}$ is shown in the Fig 15. Two Sharp and intense peaks appeared at $416 cm^{-1}$ and 403.6 cm^{-1} which are attributed to the asymmetric and symmetric stretch of Ce-O in the perovskite structure[66]. The Y-O vibrational bands also appear in the same region as in the Ce-O with small difference. Therefore the FT-IR spectrum obtained contains the overlapped peaks. The very small intensity peaks appeared at 885 cm^{-1} and 1456 cm^{-1} are might be due the presence of some carbonate impurities. [67]

Table 4: FT-IR data of the $La_{1.0}Y_{0.2}Ce_{0.8}O_{3-\delta}$ in dry atmosphere.

Experimental υ(cm-1)	species	Reported υ(cm-1)
416	Ce-O(asym)	
404	Ce-O(sym)	<500
885.1 1456	Impurities	

FT-IR spectroscopy is an important technique to determine the proton defects in the electrolyte material. Under moist conditions the proton defects are produced in the electrolyte membrane by the chemical diffusion of water[68]. FT-IR spectrum in the Fig. 16 shows the presence of these proton defects in the electrolyte membrane under moist conditions. The peaks due to the presence of M-O bond are also shifted towards the lower frequency due to the lengthening of the M-O bonds which occurs when proton

attach to the oxygen atom. Hence M-O-H bond will absorb at lower frequency than the M-O bond. Therefore the Ce-O bond undergo a red shift from 416 cm^{-1} to 412 cm^{-1}[66]. Thus FT-IR is a valuable technique to characterize the ceramic electrolyte membranes for their proton defects retention power even after the long time of exposure to humid air.
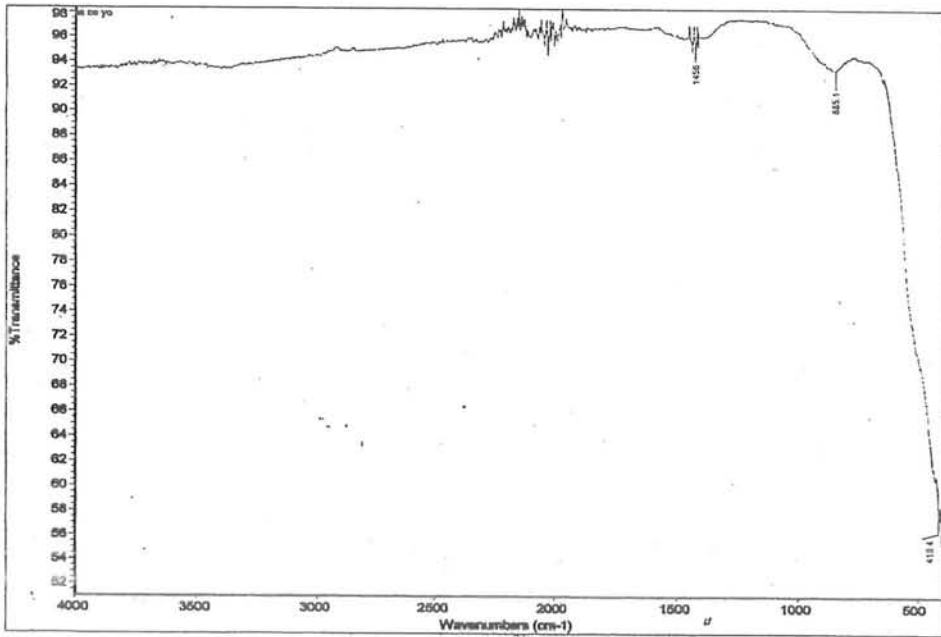
Figure 15: FT-IR spectrum of $La_{1.0}Y_{0.2}Ce_{0.8}O_{3-\delta}$ obtained at T=1050°C

The FT-IR data of $La_{1.0}Y_{0.2}Ce_{0.8}O_{3-\delta}$ after exposing to humid air is given in the Table 15.

Table 5: FT-IR data of the $La_{1.0}Y_{0.2}Ce_{0.8}O_{3-\delta}$ (after exposure to humid air).

Experimental υ(cm-1)	species	Reported υ(cm-1)
3321(After exposure of material to humid air)	O-H(s)	3300-3400
412	Ce-O(asym)	<500
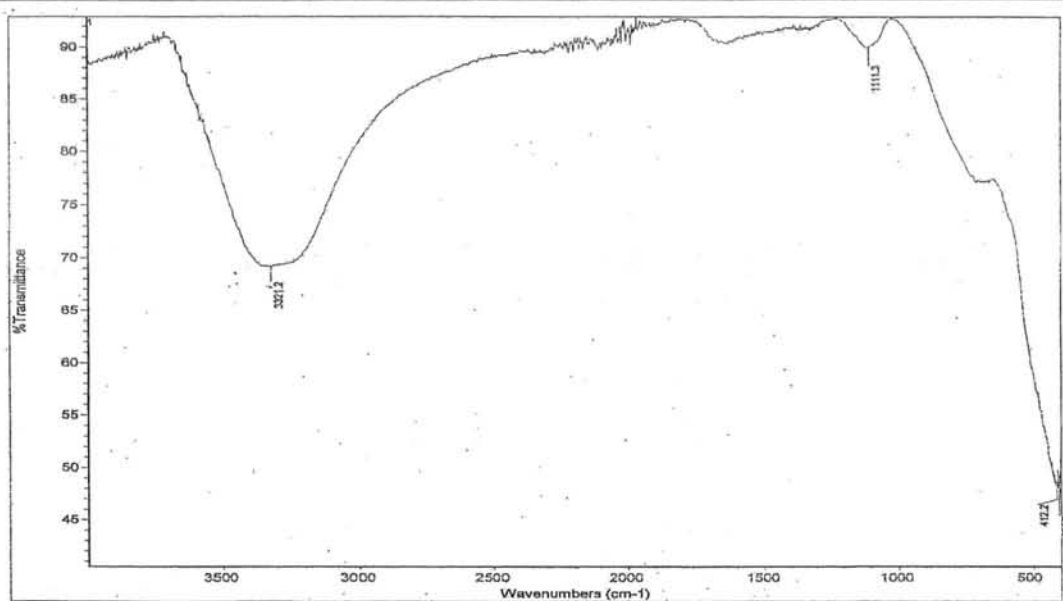
Figure 16: FTIR spectrum of $La_{1.0}Y_{0.2}Ce_{0.8}O_{3-\delta}$ in O-H stretching regime.

The presence of oxygen vacant sites, formation of proton defects under moist conditions and high conductivity in moist air make $La_{1.0}Y_{0.2}Ce_{0.8}O_{3-\delta}$ a suitable material to act as proton conducting electrolyte membrane for the solid oxide fuel cell. These membranes can also be used in the extraction of hydrogen gas from the mixture of different gases.

2. Characterization of $Ba_{1.0}Y_{0.2}Ce_{0.8}O_{3-\delta}$

2.1 X-ray diffraction pattern
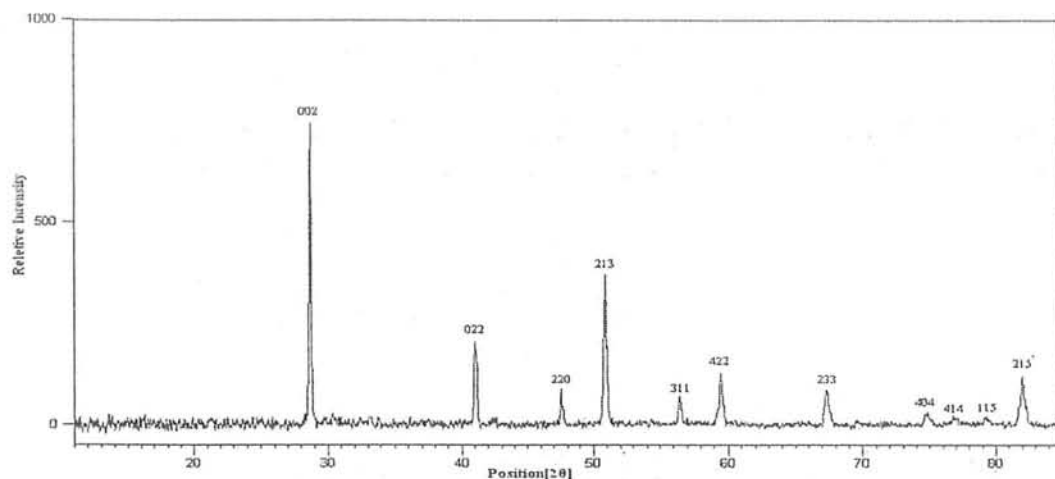
Figure 17: X-Ray diffraction pattern of $Ba_{1.0}Y_{0.2}Ce_{0.8}O_{3-\delta}$ calcined at $1050^{\circ}C$

The crystal structure of the calcined oxide powder was determined by X-ray diffraction (XRD) analysis using a PANalytical X-ray diffractometer (monochromated Cu Kα radiation, λ=0.15418nm; operated at 40KV) at room temperature in the bragg angle range of 10° to 90°. Two peaks of very small intensity appeared for CeO_2 even after calcining at $T=1050^{\circ}C$ which indicate tat a small amount of Ce forms a separate phase. Rest of the peaks are indexed to miller indices and show a good match with the standard peak pattern of the ICDD card 01-081-1386 as shown in the Fig 18. X-ray diffraction data shows that the ceramic material $Ba_{1.0}Y_{0.2}Ce_{0.8}O_{3-\delta}$ is single phase with orthorhombic crystal structure having space group Pmcn. The cell parameters including the edge length and bond angles and all other informations regarding the crystal system, space group, cell volume etc. are given in the Table 7.
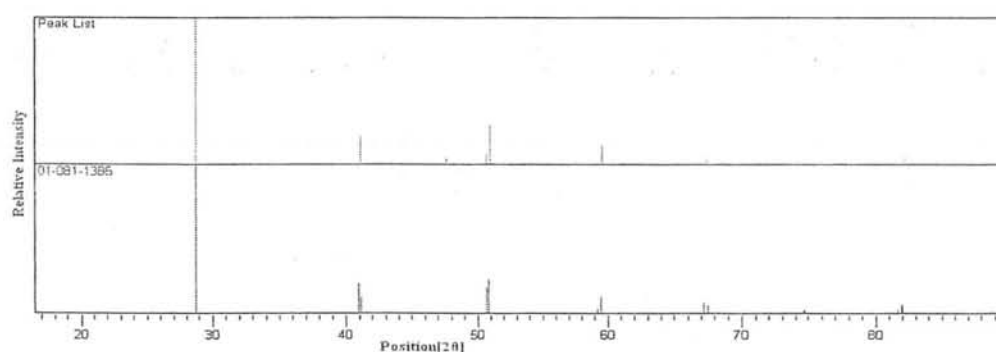
Figure 18: Comparison of peak pattern of the $Ba_{1.0}Y_{0.2}Ce_{0.8}O_{3-\delta}$ with the standard peak pattern.

The particle size of the ceramic electrolyte material is 33nm which is calculated using the Scherrer,s formula.

Table 6: Powder x-ray diffraction data of the decomposed material $Ba_{1.0}Y_{0.2}Ce_{0.8}O_{3-\delta}$

Parameters		$Ba_{1.0}Y_{0.2}Ce_{0.8}O_{3-\delta}$ [01-081-1386]		
Crystal System		Orthorhombic		
Space group		Pmcn		
Cell Volume (10^6pm^3)		340.55		
Z		4.00		
Cell parameters		$a=8.7705$Å $\alpha=\beta=\gamma=90.00°$ $b=6.2393$Å $c=6.2233$Å		
No.	Position [°2θ]	d-spacing	hkl match with	
			$Ba_{1.0}Ce_{0.8}Y_{0.2}O_3$	CeO_2
1.	28.698	3.10821	002	
2.	40.931	2.20309	022	
3.	47.835	1.90000	-----	220
4.	50.800	1.79585	213	
5.	56.783	1.62000	-----	311
6.	59.426	1.55411	422	
7.	67.160	1.39269	233	
8.	74.758	1.26885	404	
9.	76.561	1.24340	414	
10.	79.161	1.20896	115	
11.	81.897	1.17535	215	

2.2 Energy Dispersive X-ray Analysis of $Ba_{1.0}Y_{0.2}Ce_{0.8}O_{3-\delta}$

Energy dispersive x-ray analysis of the $Ba_{1.0}Y_{0.2}Ce_{0.8}O_{3-\delta}$ proves that elemental ratio in agreement with the expected values.
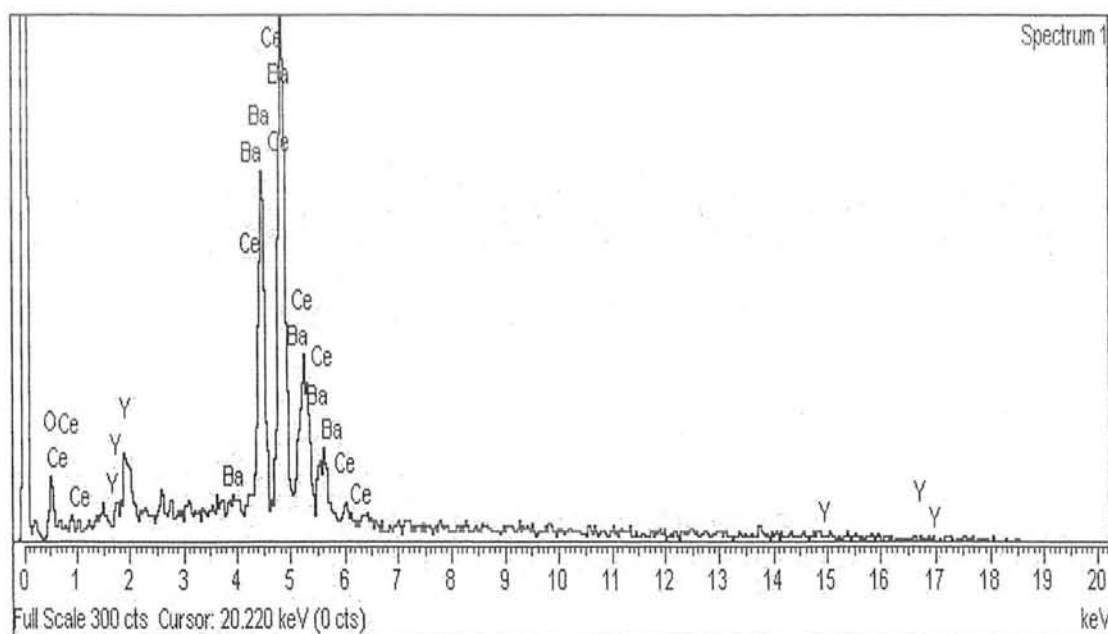
Figure 19: EDX spectrum of the $Ba_{1.0}Y_{0.2}Ce_{0.8}O_{3-\delta}$

The elemental ratio calculated from the data given by the EDX graph is shown in Table 7.

Table 7: Elemental ratio of the $Ba_{1.0}Y_{0.2}Ce_{0.8}O_{3-\delta}$

Elements	Elemental Ratio(W%)	Molar Ratio
Ba	45.37	0.991
Ce	36.64	0.782
Y	6.19	0.208
O	11.80	2.211

EDX data of the $Ba_{1.0}Y_{0.2}Ce_{0.8}O_{3-\delta}$ shows that it is oxygen deficient ceramic material. 2.21mmol of the oxygen are present in the material while almost 3mmol should be present for complete structure without any oxygen deficiency.

Scanning electron micrograph of the $Ba_{1.0}Y_{0.2}Ce_{0.8}O_{3-\delta}$ shows a good surface morphology. The material has coarse surface with the homogeneous distribution of the particles. The particles have clearly well defined boundaries and smooth surface.

38
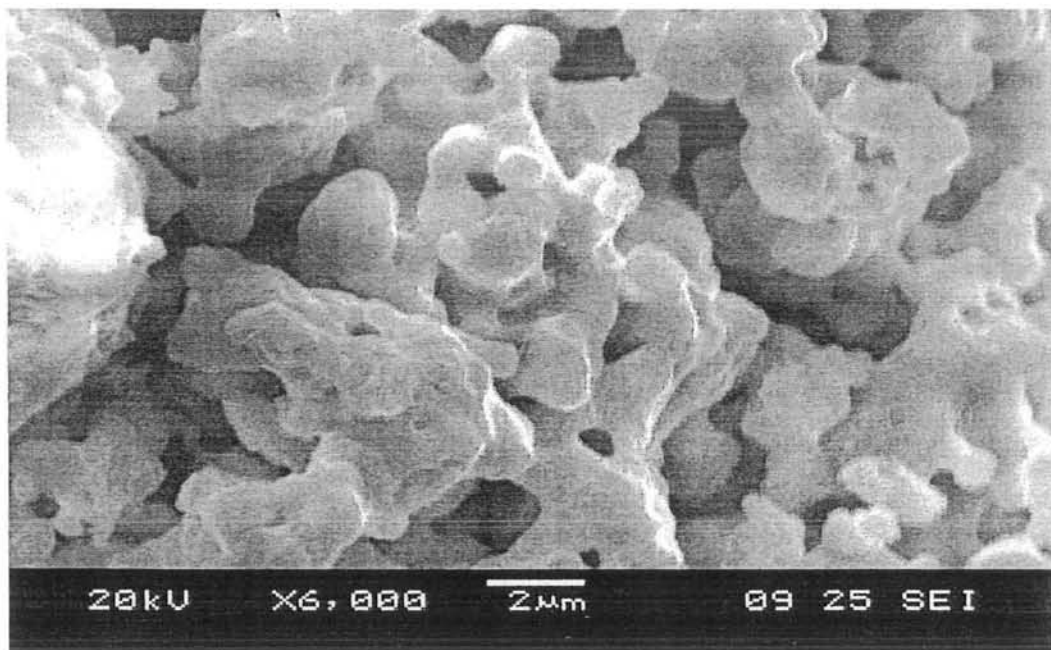
Figure 20: SEM micrograph of the $Ba_{1.0}Y_{0.2}Ce_{0.8}O_{3-\delta}$

2.3 Thermogravimetric Analysis (TGA) of $Ba_{1.0}Y_{0.2}Ce_{0.8}O_{3-\delta}$

2.3.1 Thermogravimeteric analysis in O_2 atmosphere

Thermal analysis of $Ba_{1.0}Y_{0.2}Ce_{0.8}O_{3-\delta}$ in open air shows that weight of the material increases with the increase in temperature continuously. $Ba_{1.0}Y_{0.2}Ce_{0.8}O_{3-\delta}$ is a complex perovskite ceramic material in which Ce(IV) is partially doped with the Y(III). Due to the replacement of the higher oxidation state metal with the lower oxidation state metal will generate the oxygen vacant sites in the material. Thus material (i.e. $Ba_{1.0}Y_{0.2}Ce_{0.8}O_{3-\delta}$) will become oxygen deficient in nature and whenever it will come in contact with the O_2 at high temperature the oxygen will enter into the vacant sites in order to remove the flaws in the structure. Thermogram of the material in Fig 21 indicates a small gain in weight on heating the material in O_2 atmosphere. The gain in weight occurs when oxygen enter into the vacant sites and reside there at high temperature. At high temperature the oxygen split into oxide ion radicals which have one electron for bonding with the metal atom. Therefore an electron hole is generated when oxygen fill the vacant site because for the complete bond formation two electrons are required to transfer to the metal atom. When oxygen get absorbe, an electron hole is also generated as shown by the following equation.

$$V_O^{\bullet\bullet} \; + \; 1/2O_2 \; \rightleftharpoons \; O_O^X \; + \; 2h^\bullet$$

The absorption of oxygen at the surface is very small therefore the weight gain is also very small as shown in the Fig. 21. The lower line is the stability line showing no weight change with that of the temperature. The upper line is the experimental line which shows that small gain in weight takes place with the increase in temperature. In the beginning of the graph the weight gain is almost negligible because the oxygen vacancies are not filled by the atmospheric oxygen at lower temperature but higher temperature the heat energy can split the atmospheric oxygen which can diffuse the into the surface of electrolyte material and fill up the oxygen vacancies and as result of this, the weight of the electrolyte material increased which also accompanied with the increase in p-type conductivity as shown in Fig. 23 due to the generation of electron holes.
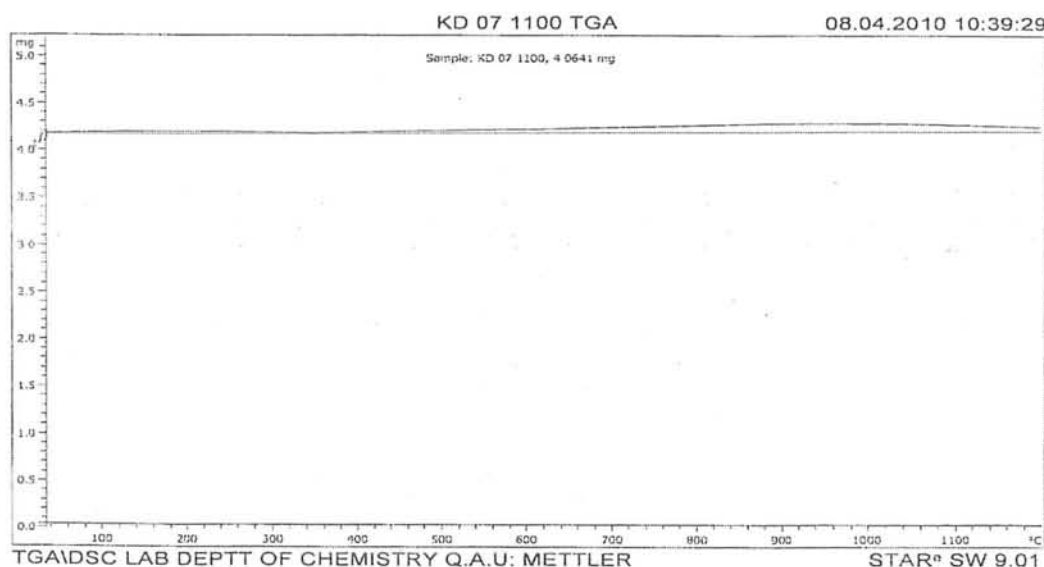
Figure 21: Thermogram of the $Ba_{1.0}Y_{0.2}Ce_{0.8}O_{3-\delta}$ in O_2 atmosphere.

Weight increment of the $Ba_{1.0}Y_{0.2}Ce_{0.8}O_{3-\delta}$ calculated from the thermogram is given in the Table 8.

Table 8: weight gain by the $Ba_{1.0}Y_{0.2}Ce_{0.8}O_{3-\delta}$ at high temperature and O_2 atmosphere.

Initial weight	Final Weight	Weight Increment (%)
4.18mg	4.28mg	2.39

2.3.2 Termogravimeteric analysis of $Ba_{1.0}Y_{0.2}Ce_{0.8}O_{3-\delta}$ in N_2 atmosphere.

Thermogravimetric analysis done in the nitrogen atmosphere is shown in the Fig 22. Thermogram shows that material is highly stable in nitrogen atmosphere and weight gain or loss is almost zero. It means that $Ba_{1.0}Y_{0.2}Ce_{0.8}O_{3-\delta}$ is non reactive towards nitrogen even at very high temperature and also it is very stable ceramic material which is not decomposed at high temperature. $Ba_{1.0}Y_{0.2}Ce_{0.8}O_{3-\delta}$ is reactive towards the oxygen and water vapors at high temperature. When oxygen absorbed into the vacant sites electron holes are generated due to which the material shows p-type conductivity and when water vapors are absorbed the proton defects are formed as shown in FT-IR spectrum of $Ba_{1.0}Y_{0.2}Ce_{0.8}O_{3-\delta}$ in Fig 26 due to which the material becomes proton conducting in nature and show high conductivity in moist air as shown in Fig. 24.
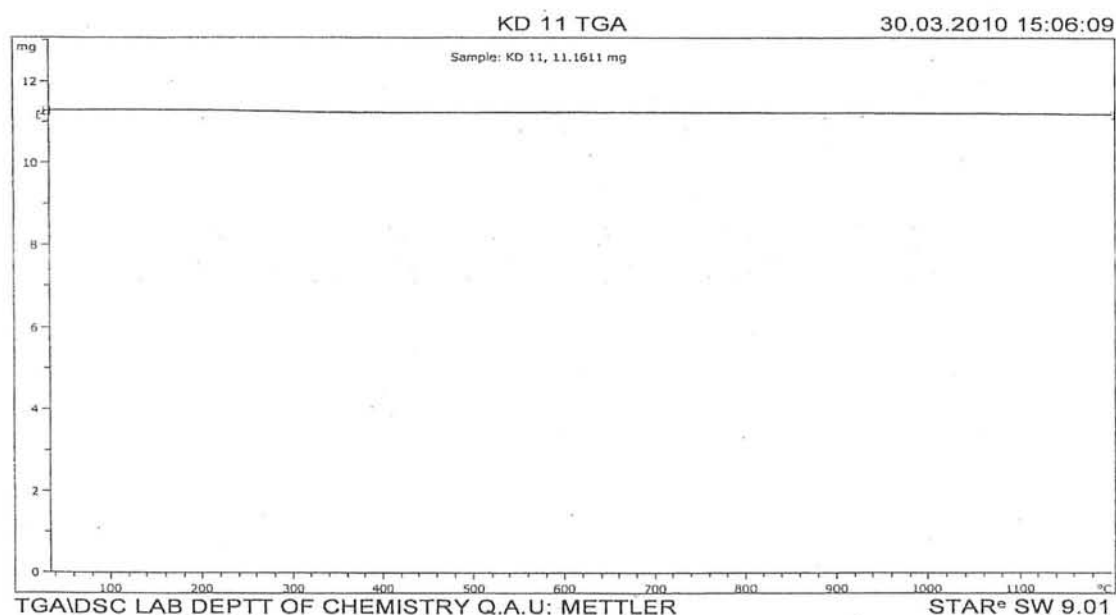
Figure 22: Thermogram of the $Ba_{1.0}Y_{0.2}Ce_{0.8}O_{3-\delta}$ in N_2 atmosphere.

2.4 Electrical conductivity measurement of $Ba_{1.0}Y_{0.2}Ce_{0.8}O_{3-\delta}$

The electrical conductivity of the electrolyte ($Ba_{1.0}Y_{0.2}Ce_{0.8}O_{3-\delta}$) was determined using the electrical conductivity meter (Keithley-2400 USA), temperature sensing multimeter and the tube furnace (carbolyte UK). Green colored pallet of the electrolyte material was kept between the jaw like electrodes of the conductivity meter. The electrodes

containing pallet and temperature sensing probe were kept in the tube of the tube furnace. The conductivity as a function of temperature was recorded in the temperature range of 30°C to 750°C with 5°C temperature difference. The conducting behavior of the electrolyte material as a function of temperature is shown in the Fig 23.

$Ba_{1.0}Y_{0.2}Ce_{0.8}O_{3-\delta}$ is best proton conductors [69]. For a material to act as electrolyte for the solid oxide fuel cell it should be a good ionic conductor and resistor for the electron movement. It is clear from the conductivity graph that electrolyte can conduct the electrical current only slightly and overall it is resistive material. The material (i.e. $Ba_{1.0}Y_{0.2}Ce_{0.8}O_{3-\delta}$) contains oxygen vacancies which are produced in the material in order to compensate the acceptor dopant which is yttrium (III) in our case. The mobility of protonic defects is very sensitive not only towards local structural and chemical perturbations induced by the acceptor dopant but also by the mixed occupancy on the B-site [69]. The oxygen vacancies are necessary for the formation of proton defects in the presence of moisture. Water in the gaseous phase split into hydroxide ion and a proton. The hydroxide ion fills the oxygen vacant sites and proton attaches to the structural oxygen, thus two positively charged proton defects are produced but in the absence of sufficient amount of moisture the proton defects are not formed and the conductivity shown by the material is due the presence of electron holes, and oxide ions.
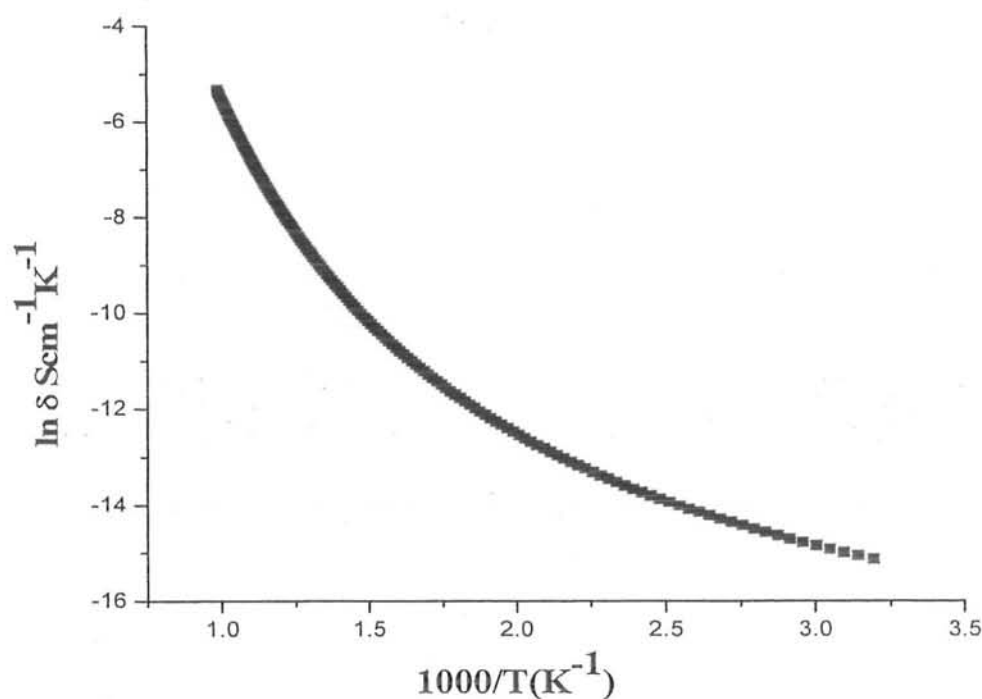

Figure 23: Arrhenius plot for electrical Conductivity of $Ba_{1.0}Y_{0.2}Ce_{0.8}O_{3-\delta}$ electrolyte

Activation energy calculated for the above mentioned arrhenius plot is 0.41eV.

Oxygen vacancies present at the surface of electrolyte are filled by the atmospheric oxygen when the atmosphere is dry. Oxygen absorption accompanied the formation of holes as shown follows.

$$V_O^{\bullet\bullet} \;+\; 1/2O_2 \;\rightleftharpoons\; O_O^X \;+\; 2h^{\bullet}$$

The oxygen ions and electron holes move across the electrolyte bulk at high temperature and conduct electricity. The filling of oxygen vacancies can be traced by recording the weight of the material as a function of temperature in open air as shown in Fig. 21. A small gain in weight of electrolyte with increase in temperature is a clear indication of the fact that oxygen vacancies are filled continuously with increase in temperature. Thus in dry atmosphere the electron holes are the charge carriers which are assisted with the oxide ions to conduct electricity. In the presence of sufficient amount of moisture the proton defects are formed and proton conductivity prevail all other conductivities i.e. conductivity due to electrons, electron holes and oxide ions because when the proton source (H_2O/H_2) is available, the equilibrium shown in above equation is shifted towards the left side. Therefore the electron hole conductivity is much less in the reducing atmosphere and the conductivity is called ionic as a whole [70]. Thus at high temperature and in dry atmosphere the material shows oxide ions and electron hole conductivity. At the low temperature the conductivity of the electrolyte material is very small.

Now if we compare the electrical conductivities of the $Ba_{1.0}Y_{0.2}Ce_{0.8}O_{3-\delta}$ in dry air and moist air environments, the conduction behavior boost up in the moist environment while in the dry air the conductivity is very small as shown in the Fig. 24. $Ba_{1.0}Y_{0.2}Ce_{0.8}O_{3-\delta}$ is oxygen deficient perovskite electrolyte material, when encounter water vapors; the water molecules split into protons and hydroxide ions. Protons form covalent bond with the structural oxygen atom while the hydroxide ion reside into the oxygen vacant site present in the $Ba_{1.0}Y_{0.2}Ce_{0.8}O_{3-\delta}$, as a result proton defects are produced in the electrolyte membrane. Once the proton defects are produced the conductivity due to the protons overrides the electron hole conductivity. Therefore the conductivity in moist air environment is the purely ionic conductivity which occurs because of the chemical diffusion of water in the bulk of electrolyte membrane. Protons

43

are very small in size and require much less enthalpy for long range diffusion across the bulk of the electrolyte membrane while oxide ions need higher enthalpy and activation energy for their movement trough the electrolyte membrane. Therefore the electrolyte membrane ($Ba_{1.0}Y_{0.2}Ce_{0.8}O_{3-\delta}$) showed the much higher conductivity in moist air then in dry air at $600^{\circ}C$ i.e. the electrolyte membrane can work efficiently at moderate temperature and in sufficiently wet atmosphere. At much higher temperature the conductivity due to oxide ions become prominent in dry conditions as shown in the Fig. 22, but whenever the water partial pressure increases the proton conductivity dominate all other conductivities.
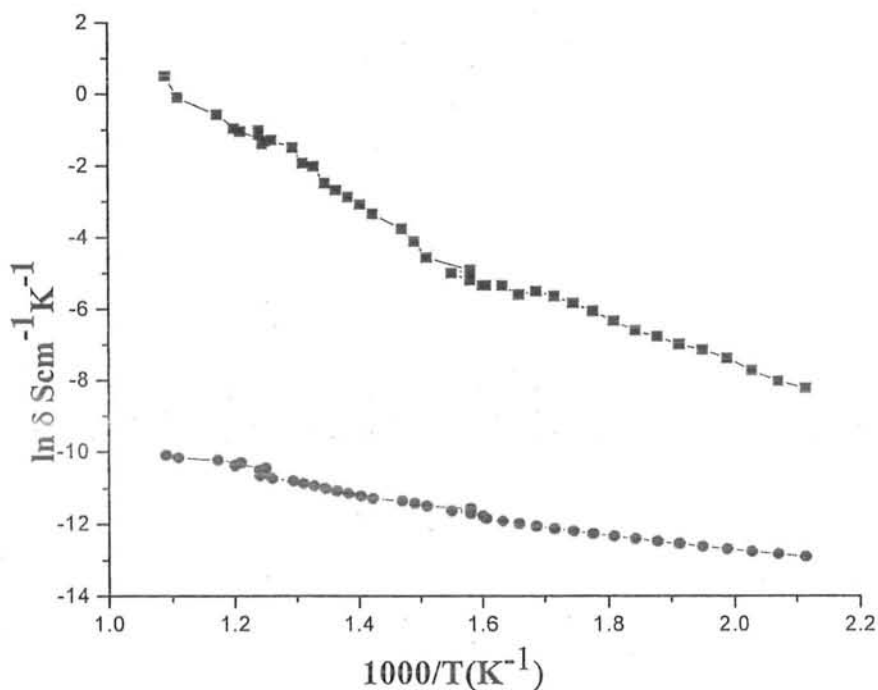
Figure 24: comparison of ionic conductivities of $Ba_{1.0}Y_{0.2}Ce_{0.8}O_{3-\delta}$ in dry air (I) and moist air (II) at $T=300-600^{\circ}C$.

Thus the operational temperature for the proton conducting solid oxide fuel cell lie in the range of $300-600^{\circ}C$ while the conventional oxide ion conducting solid oxide fuel cells work better in the temperature range of $800-1000^{\circ}C$ because the oxide ions need more enthalpy for long range conduction through the electrolyte membrane as compare to the protons. Hence proton conducting SOFC are more advantageous than

conventional oxide ion conducting SOFC due to high efficiency and less working temperature.

2.5 FT-IR analysis of $Ba_{1.0}Y_{0.2}Ce_{0.8}O_{3-\delta}$.

FT-IR of the electrolyte material was done with the Fourier transform infra red spectrophotometer of model thermo scientific (Nicolet-6700). Two peaks appear at 430.0 cm^{-1} and 403.2 cm^{-1}. These peaks are attributed to the asymmetric and symmetric stretch of O-Ce bond[66]. A very small peak appear at 885 cm^{-1} which might be due to the presence of carbonate bending vibrations[67].

Table 9: FT-IR data of the $Ba_{1.0}Y_{0.2}Ce_{0.8}O_{3-\delta}$ in dry air.

Observed peaks υ(cm-1)	Species	Reported υ(cm-1)
430.0	Ce-O(asym)	
403.2	Ce-O(sym)	<500
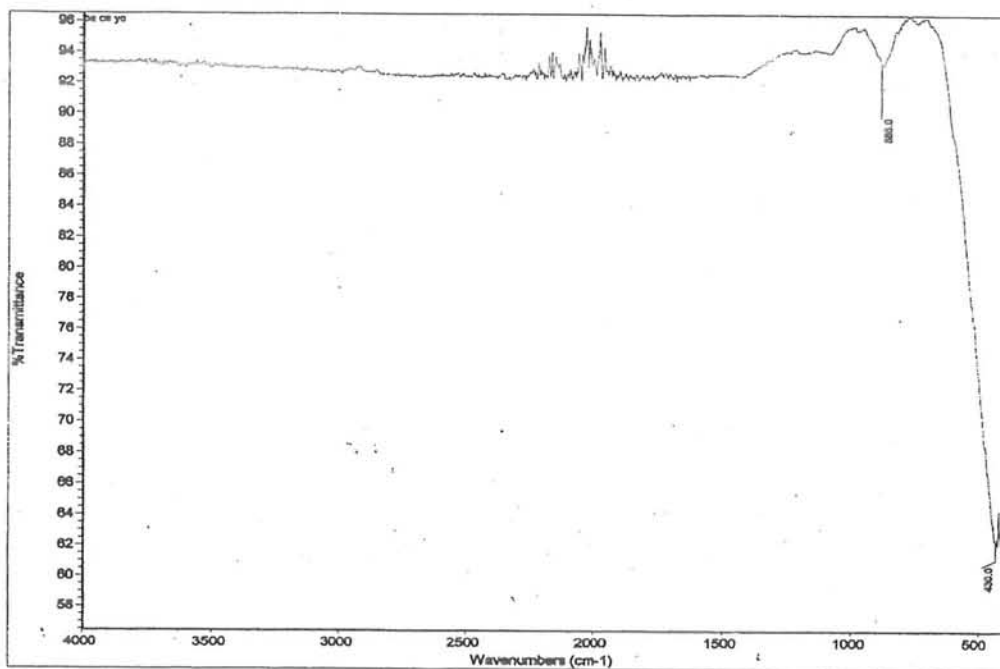
Figure 25: FTIR spectrum of the $Ba_{1.0}Y_{0.2}Ce_{0.8}O_{3-\delta}$ in dry atmosphere.

When $Ba_{1.0}Y_{0.2}Ce_{0.8}O_{3-\delta}$ was exposed to the humid air the proton defects were produced which are evidenced by the appearance of a broad band at 3345.2 cm^{-1}[68] which indicates the presence of O-H species in the electrolyte material.

Table 10: FT-IR data of the $Ba_{1.0}Y_{0.2}Ce_{0.8}O_{3-\delta}$. After exposure to humid air.

Observed peaks υ(cm-1)	species	Reported υ(cm-1)
3345.2	O-H(s)	3300-3400
423.0	Ce-O(s)	<500
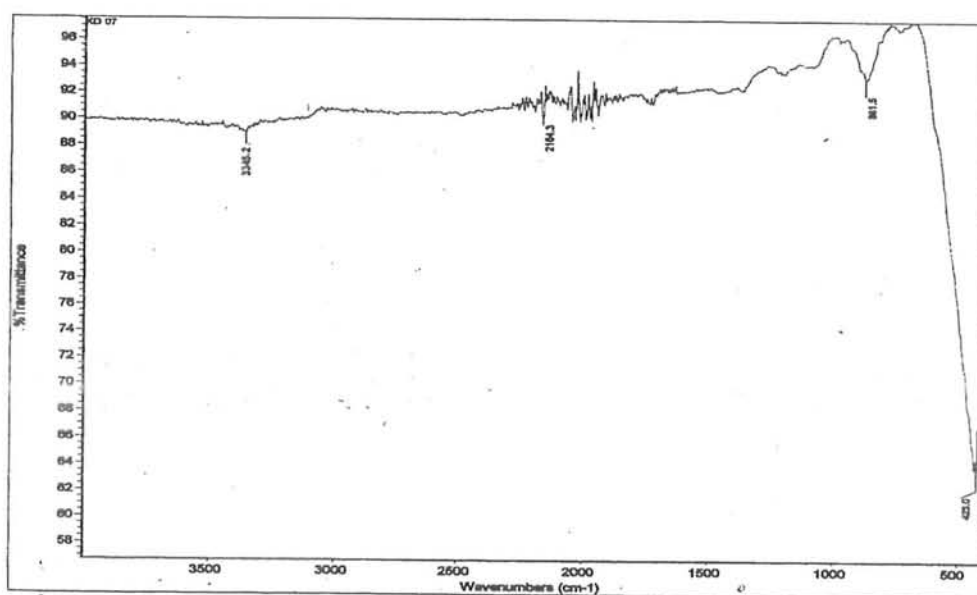
Figure 26: FT-IR spectrum of $Ba_{1.0}Y_{0.2}Ce_{0.8}O_{3-\delta}$ (after exposure to humid air)

3. XRPD Analysis of $Sr_{1.0}Y_{0.2}Zr_{0.8}O_{3-\delta}$

3.1 X-Ray diffraction pattern
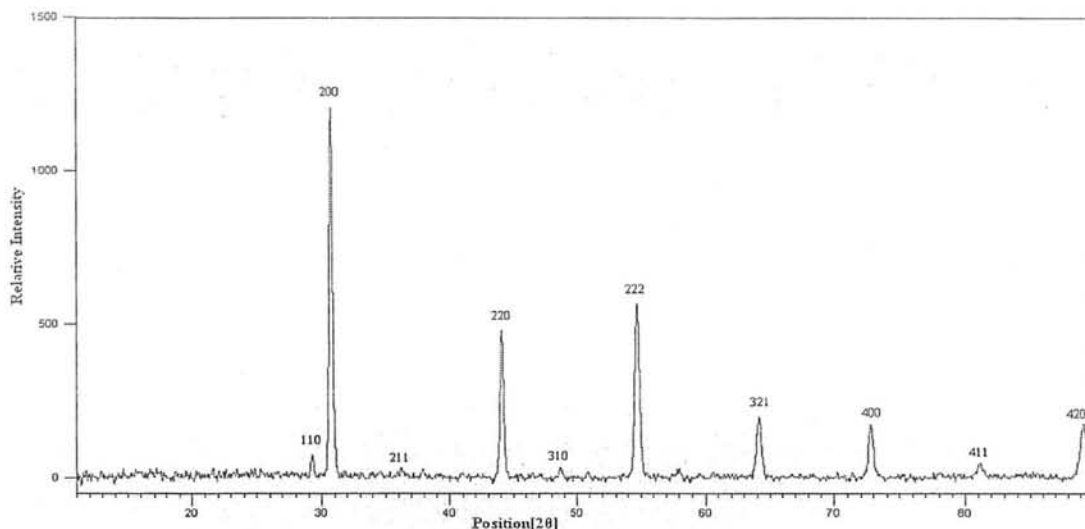
Figure 27: X-ray diffraction pattern of the $Sr_{1.0}Y_{0.2}Zr_{0.8}O_{3-\delta}$

The crystal structure of the calcined powder electrolyte was determined by XRD analysis. The pattern shows that the material is single phase crystalline in nature with the cubic structure. The particle size is 43.08nm according to the Scherrer,s formula.

Peak pattern of the $Sr_{1.0}Y_{0.2}Zr_{0.8}O_{3-\delta}$ showed a good match with that of the standard values of ICDD card 00-051-0254 as shown in the Fig. 28. Some small intensity peaks are deviated from their position. It is due to the difference in the chemical composition of the two materials. The standard material has chemical composition $Sr_2ZrY_{0.5}O^{[71]}$ while in our case the material has different ratio among the elements i.e, $Sr_{1.0}Y_{0.2}Zr_{0.8}O_{3-\delta}$.
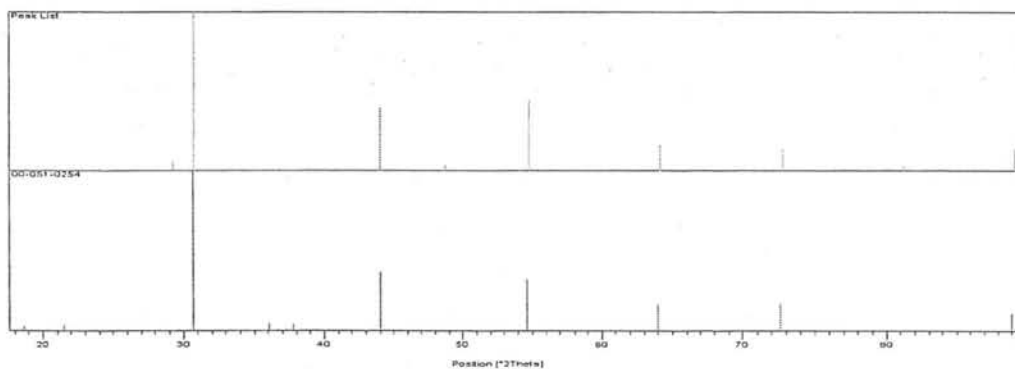
Figure 28: Comparison of the peak pattern of $Sr_{1.0}Y_{0.2}Zr_{0.8}O_{3-\delta}$ with standard peak pattern.

47

3.2 Energy Dispersive X-ray Analysis of $Sr_{1.0}Y_{0.2}Zr_{0.8}O_{3-\delta}$

EDX spectrum of the $Sr_{1.0}Y_{0.2}Zr_{0.8}O_{3-\delta}$ is shown in Fig. 29. The elemental ratio calculated from the EDX data show a good agreement with the standard values used for the reaction.
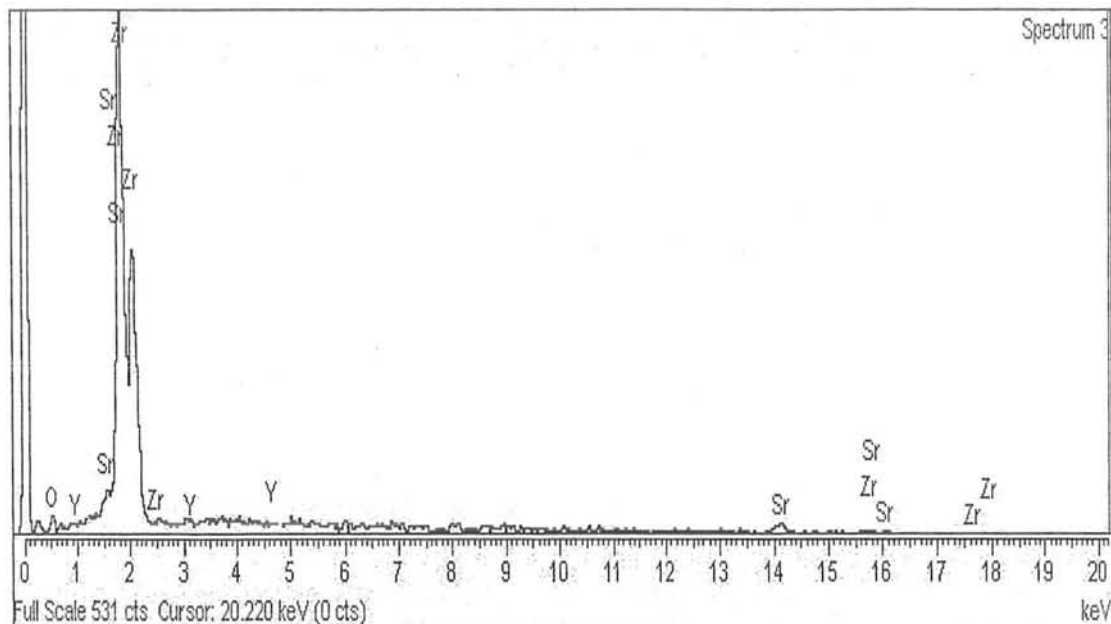
Figure 29: EDX spectrum of the $Sr_{1.0}Y_{0.2}Zr_{0.8}O_{3-\delta}$

The functional properties of the material depend upon the phase purity of the material, desired ratio among different elements, and homogeneity of the particle distribution and all these characters come from the sophistication of the synthetic methods adopted for the fabrication of the ceramic material. Results of analytical techniques i.e, XRPD, EDX and SEM indicate that material is single phase with homogeneous particle distribution having the elemental ratio almost same as required. Thus it is the novelty of the solution method for synthesis of ceramic materials with best characteristics.

Elemental ratio calculated from the data provided by the energy dispersive X-ray analysis is shown in the table. Oxygen is some what less than the required quantity from which we infer that the $Sr_{1.0}Y_{0.2}Zr_{0.8}O_{3-\delta}$ is oxygen deficient, which make it good material for ionic conduction because ionic conductivity depends upon the presence of oxygen vacant sites in the material.

Table 11: Elemental ration of the $Sr_{1.0}Y_{0.2}Zr_{0.8}O_{3-\delta}$

Elements	Elemental Ratio (W%)	Molar Ratio
Sr	42.08	0.96
Zr	33.74	0.82
Y	8.28	0.198
O	15.90	2.78

EDX data shows that material is decomposed without formation of carbonates which means that electrolyte materials prepared by the solution method are pure enough that we can use them for different technological applications.
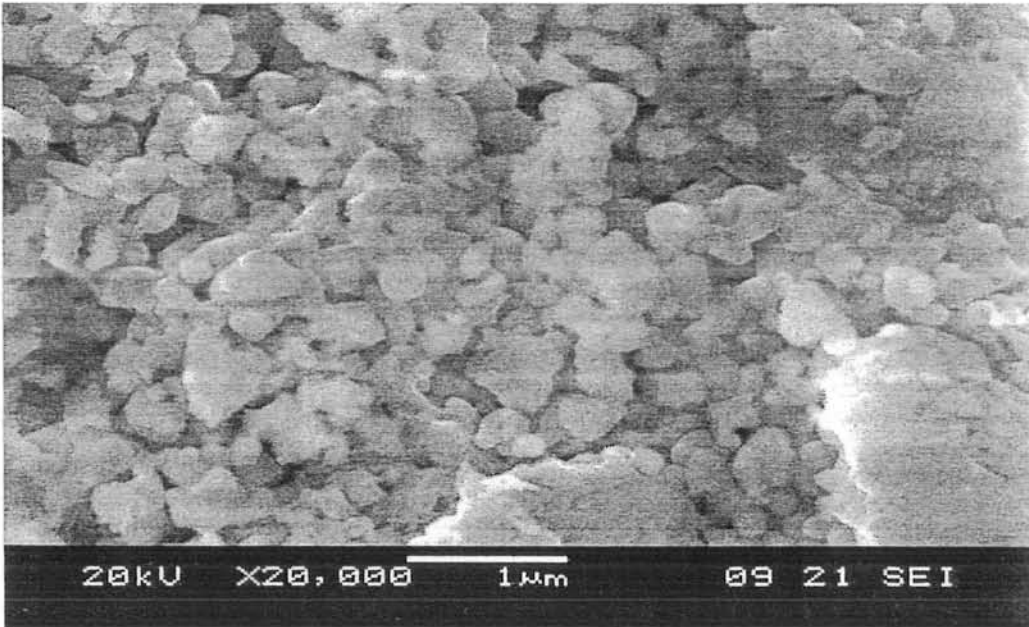
Figure 30: SEM micrograph of the $Sr_{1.0}Y_{0.2}Zr_{0.8}O_{3-\delta}$

Scanning electron micrograph (SEM) of the $Sr_{1.0}Y_{0.2}Zr_{0.8}O_{3-\delta}$ shows that material has coarse surface morphology with homogeneous particle distribution. The particles have clearly well defined grain boundaries with good orientation.

3.3 Conductivity measurement of $Sr_{1.0}Y_{0.2}Zr_{0.8}O_{3-\delta}$

$Sr_{1.0}Y_{0.2}Zr_{0.8}O_{3-\delta}$ is a good electrolyte material for solid oxide fuel cell. It has high stability even under drastic conditions of oxidation and reduction. strontium is an

alkaline earth metal existing in oxidation state of +2 present at the site A in the structure and Zirconium is the transition metal having oxidation state +4 occupy the site B in the perovskite material and is partially replaced with the Y(III) as acceptor dopant. For the perovskites ceramic materials acceptor dopant is essential for the proton conduction to take place.

Figure 31: Cubic structure of the doped perovskite.
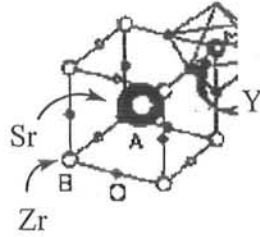
Replacement of Zr(IV) with Y(III) result in the formation of oxygen vacant sites in the material. Due to the presence of oxygen vacant sites the material become conductor when heated at higher temperature as shown in Fig. 32.
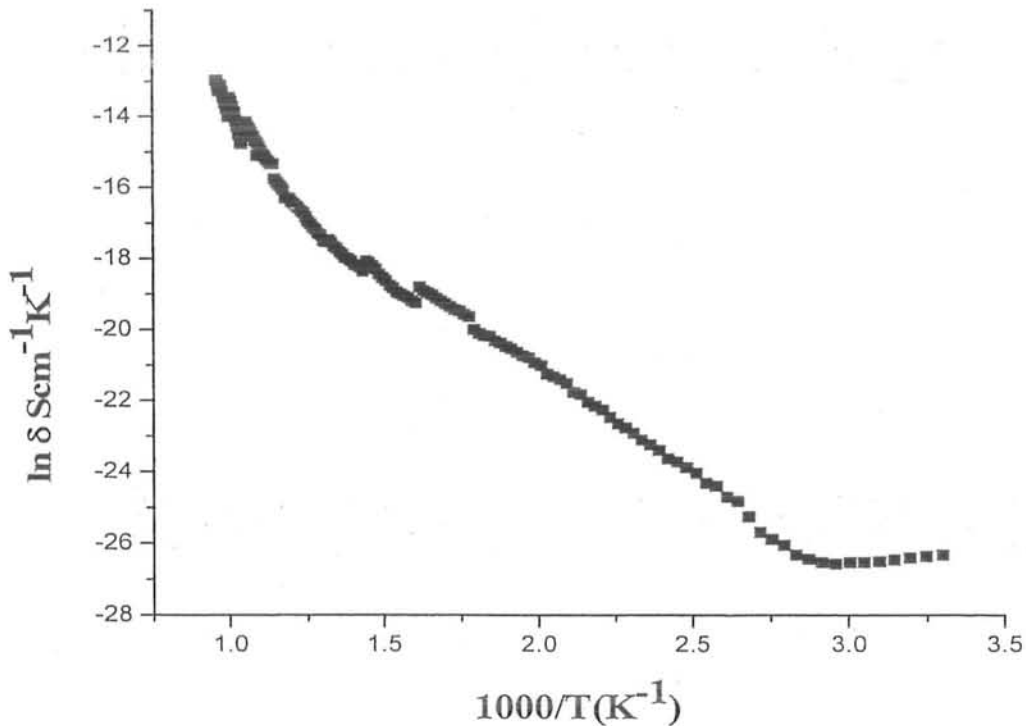
Figure 32: Arrhenius plot of electrical conductivity of $Sr_{1.0}Y_{0.2}Zr_{0.8}O_{3-\delta}$ as a function of the temperature with Ea=0.57eV

Conductivity of $Sr_{1.0}Y_{0.2}Zr_{0.8}O_{3-\delta}$ is very small at room temperature but as the temperature started to increase the conductivity increased accordingly. The reasons for such type of behavior are same as has also been discussed in the previous sections that oxide ions and electron holes contribute much in the electrical conductivity of the electrolyte under the dry atmospheric conditions i.e, in O_2 atmosphere. In reducing atmosphere of hydrogen or wet air the proton conductivity accedes the oxide ions and electron holes mixed conductivity. The one reason for the high proton conduction in the reducing atmosphere is that the protons are small in size and activation energy required for rotational diffusion of protons is small but it is high for the oxide ion conduction. Therefore the oxide ion conductor fuel cells operate at the temperature 900 to 1000°C and the pure proton conducting solid oxide fuel cells require an operating temperature lower than 700°C [72].

Under moist air condition water vapors which come into contact with the membrane surface split into protons and hydroxide ions and absorb into the membrane surface thus producing proton defects in the membrane. Due to the presence of proton defects, the electrolyte membrane become proton conductor and its conductivity boost up in the presence of moist air as shown in the Fig. 33.

Figure 33: comparison of electrical conductivities of the $Sr_{1.0}Y_{0.2}Zr_{0.8}O_{3-\delta}$ I dry air (I) and moist air (II) at T=300-600°C

$Sr_{1.0}Y_{0.2}Zr_{0.8}O_{3-\delta}$ has a large difference in the electrical conductivity in dry air and moist air environment as shown in the Fig. 33.

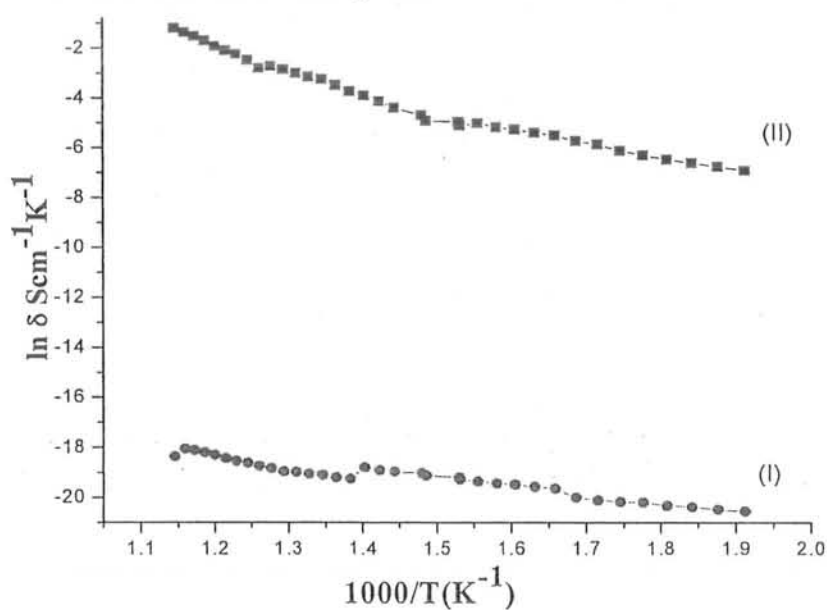The difference in the conductivities is due to the difference in the charge carrying species in two types of environments. In moist air proton defects are produced in the electrolyte membrane by the chemical diffusion of water vapors. Hence protons are the charge carrying species in the electrolyte membrane when moist air is available. Proton needs much less activation energy and enthalpy for long range diffusion through the bulk of the electrolyte membrane, and move very fast at moderate temperature. When proton get attach to the structural oxygen of the electrolyte membrane two types of forces come into action. These are the attractive forces from the negatively charged oxygen atoms and hydrogen bonding with other oxygen atoms of the membrane and second type of force which act upon the proton is repulsive force from the positively charged metal atom. Under the influence of these forces i.e. hydrogen bonding and repulsion from the metal atoms, the proton is pushed forward as illustrated in the Fig 3. Under dry conditions and at high temperature the oxygen atoms fill the oxide ion vacancies in the electrolyte membrane along with the generation of the electron holes. These oxide ions and electron holes contribute in the electrical conductivity of the electrolyte membrane.

Hence under moist conditions, protons are the charge carriers while under dry conditions the electron holes are the charge carrying species in the electrolyte membrane. Therefore the electrolyte membranes show high conductivity in moist air environment.

3.4 Thermo Gravimetric analysis (TGA) of $Sr_{1.0}Y_{0.2}Zr_{0.8}O_{3-\delta}$

TGA is a useful technique to demonstrate the effect of different environments at high temperature on the material under study. The conductivity shown by the electrolyte material in oxygen atmosphere is the direct function of the oxide ion transport number and electron holes which depends upon the absorption of oxygen from the atmosphere to fill the oxygen vacancies. An electron hole is generated in association with the oxide ion absorption. Thus at high temperature the oxide ion and electron hole conductivity is high because the oxide ion transport number increase with the temperature but the proton conduction is dominant at 700°C [73] in the presence of moist air. The quantity of

oxygen absorbed can be determined by the thermal analysis. Weight gain by the material with temperature increase is directly proportional to the quantity of oxygen absorbed. From the Fig 34 it is clear that in the beginning some loss in the weight took place which might be due to moisture or some organic species evaporation. Beyond 300°C material started to gain weight till 1100°C. This indicates that oxygen vacancies present in the sample were filled by the atmospheric oxygen at high temperature and it started beyond 300°C. From this observation we can deduce that the temperature required for the filling of oxygen vacancies present in the proton conducting perovskites is 300°C and further high temperature favors the filling up of oxygen vacancies and formation of electron holes. Thermogram of the zirconate ceramic material indicates that weight gain with temperature is very small which means that oxygen absorption is small and hence the conductivity should be small and we see from the Fig. 32, that conductivity of zirconate electrolytes is very small.
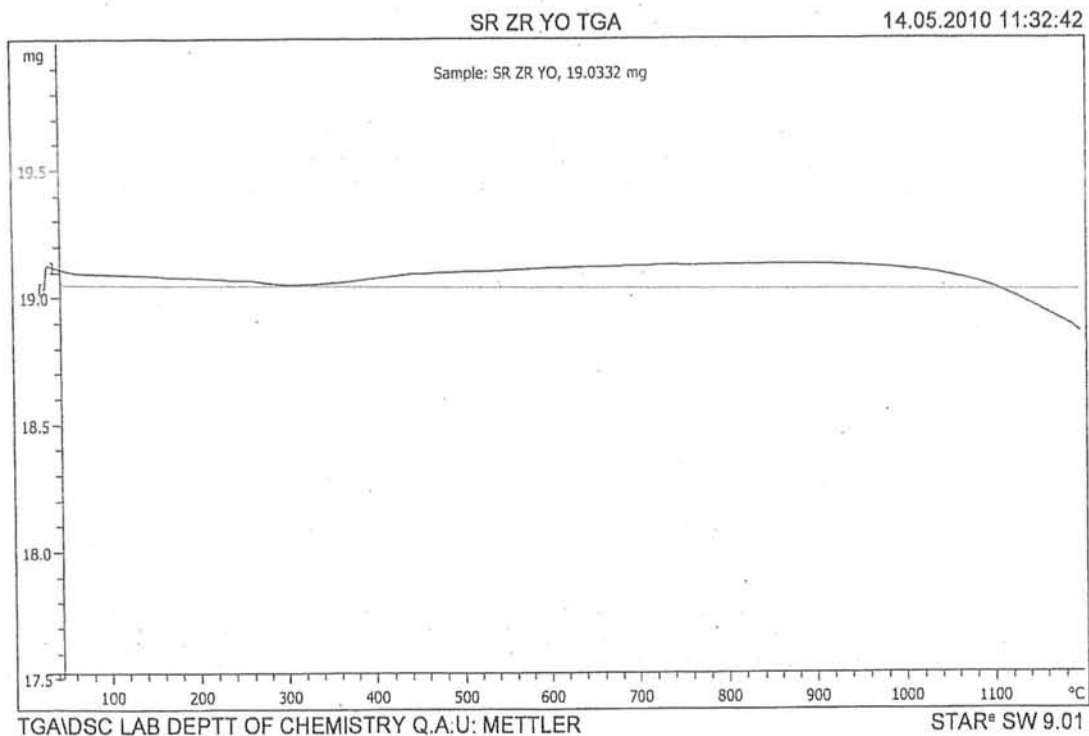
Figure 34: Thermogram of $Sr_{1.0}Zr_{0.8}Y_{0.2}O_{3-\delta}$ in air.

The change in weight of the $Sr_{1.0}Y_{0.2}Zr_{0.8}O_{3-\delta}$ membrane as a function of temperature is shown in the Table 12.

Table 12: Percent increment in the weight $Sr_{1.0}Y_{0.2}Zr_{0.8}O_{3-\delta}$ at high temperature

Initial weight	Final Weight	Weight Increment (%)
19.11mg	19.15mg	0.203

Although the weight gain is very small but it clarifies that when the material is heated in oxygen atmosphere(i.e. open air), it react with oxygen of the atmosphere at high temperature and let it to reside into the vacant sites and as a result of this absorption of oxygen the weight increases but when material is heated in the inert atmosphere of nitrogen there is no weight gain or loss take place as shown in the Fig 35. From this result we become sure about the oxygen deficient nature of the $Sr_{1.0}Y_{0.2}Zr_{0.8}O_{3-\delta}$ which is an important characteristic of the proton conducting electrolyte ceramic material.
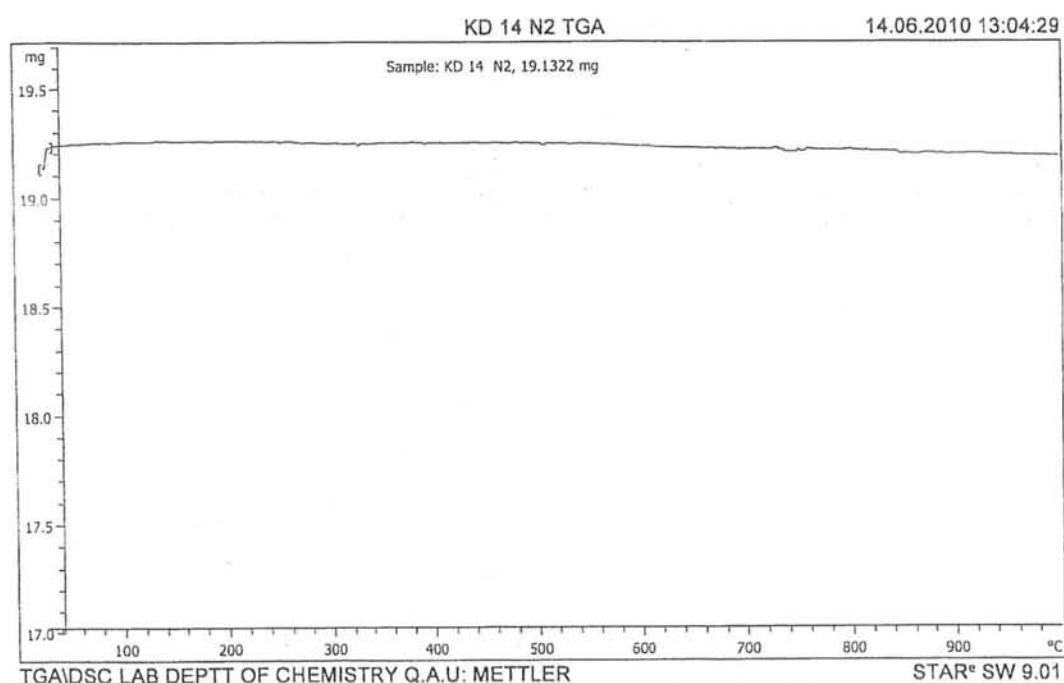
Figure 35: Thermogram of the $Sr_{1.0}Y_{0.2}Zr_{0.8}O_{3-\delta}$ in nitrogen atmosphere.

3.5 FT-IR analysis of the $Sr_{1.0}Y_{0.2}Zr_{0.8}O_{3-\delta}$

Fig 36 shows the FTIR spectrum of the powder obtained after calcination at1000°C. an intense peak appeared at 523cm^{-1} . This can be attributed to the Zr-O vibrations in the perovskite structure [74].

54

Table 13: FT-IR data of the $Sr_{1.0}Y_{0.2}Zr_{0.8}O_{3-\delta}$ in dry atmosphere

Experimental υ(cm-1)	Species	Reported υ(cm-1)
523	Zr-O(s)	537

The experimentally observed peaks appear at lower frequency as compare to the standard ones because the coordination number of the zirconium is 12 in the perovskite materials while it is two in the simple zirconium oxide material. Due to the increase in coordination number of the metal the bond lenth of M-O bond is increased which will vibrate at lower lower frequency than the simple zirconium oxide bond.
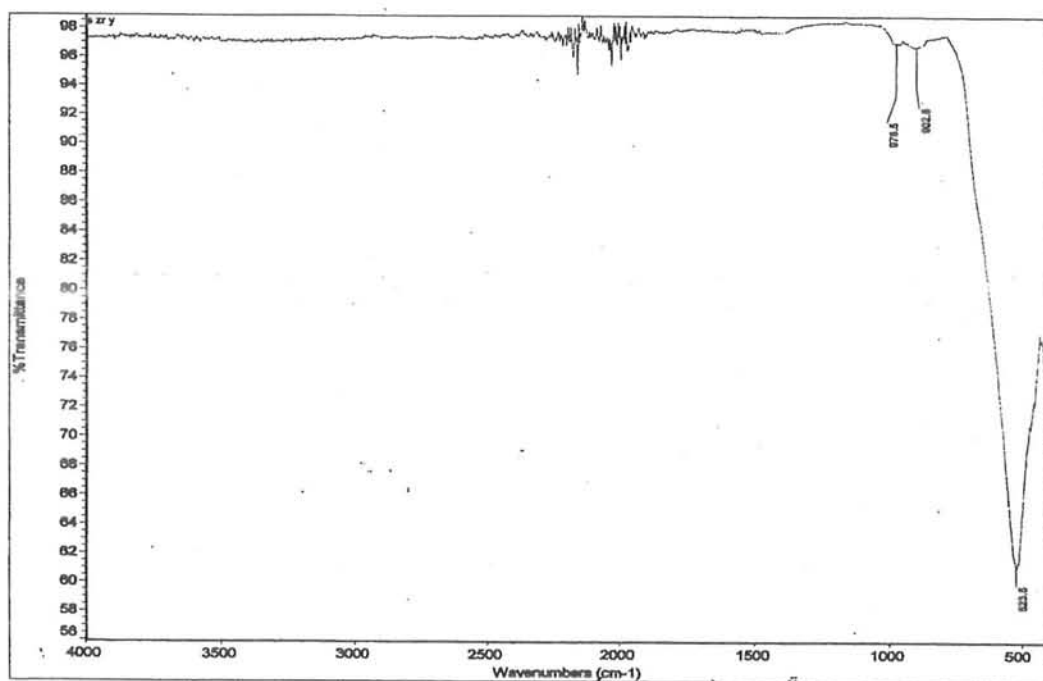
Figure 36: FT-IR spectrum of the $Sr_{1.0}Y_{0.2}Zr_{0.8}O_{3-\delta}$ in dry air.

When material was exposed to humid air the proton defects were produced in the material which were determined by the FT-IR analysis. A broad paek appeared in the O-H regime at 3400cm^{-1} which shows that hydrogen bonded O-H species are present in the $Sr_{1.0}Y_{0.2}Zr_{0.8}O_{3-\delta}$. Due the interaction of structural oxygen with that of the proton the M-O bond underwent a red shift from 523 cm^{-1} to 517cm^{-1}.
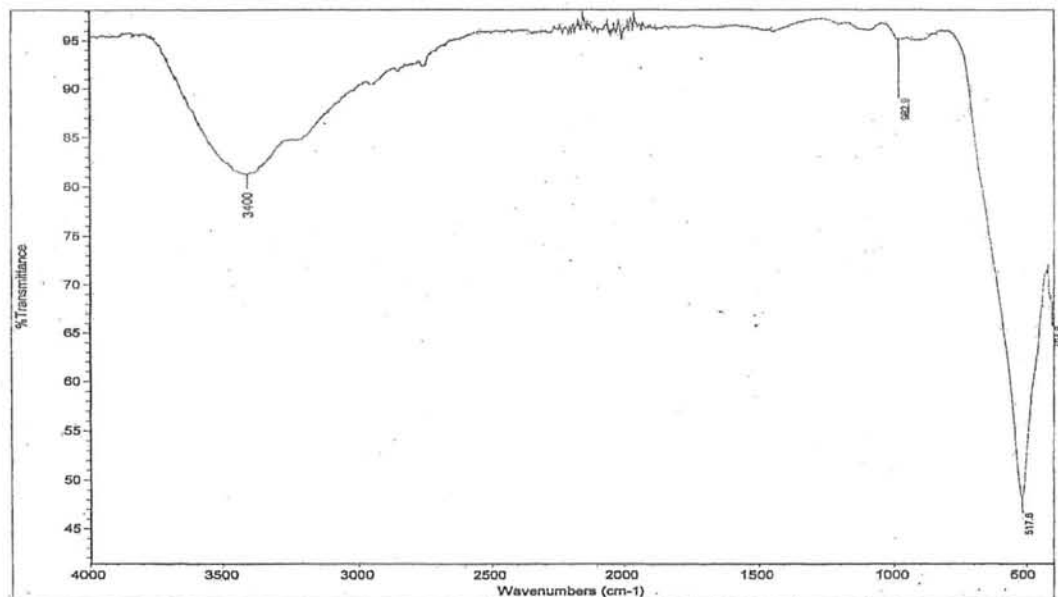
Figure 37: FT-IR spectrum of the $Sr_{1.0}Y_{0.2}Zr_{0.8}O_{3-\delta}$ in O-H stretching regime.

From the results of different analysis, it is inferred that $Sr_{1.0}Y_{0.2}Zr_{0.8}O_{3-\delta}$ is oxygen defficient material having electrical conductivity in the semiconducting range. Due to the efficient proton conducting ability in moist air this materials is regarded as a good electrolyte for the solid oxide fuel cell.

4. Comparison of electrical conductivities of electrolyte membranes
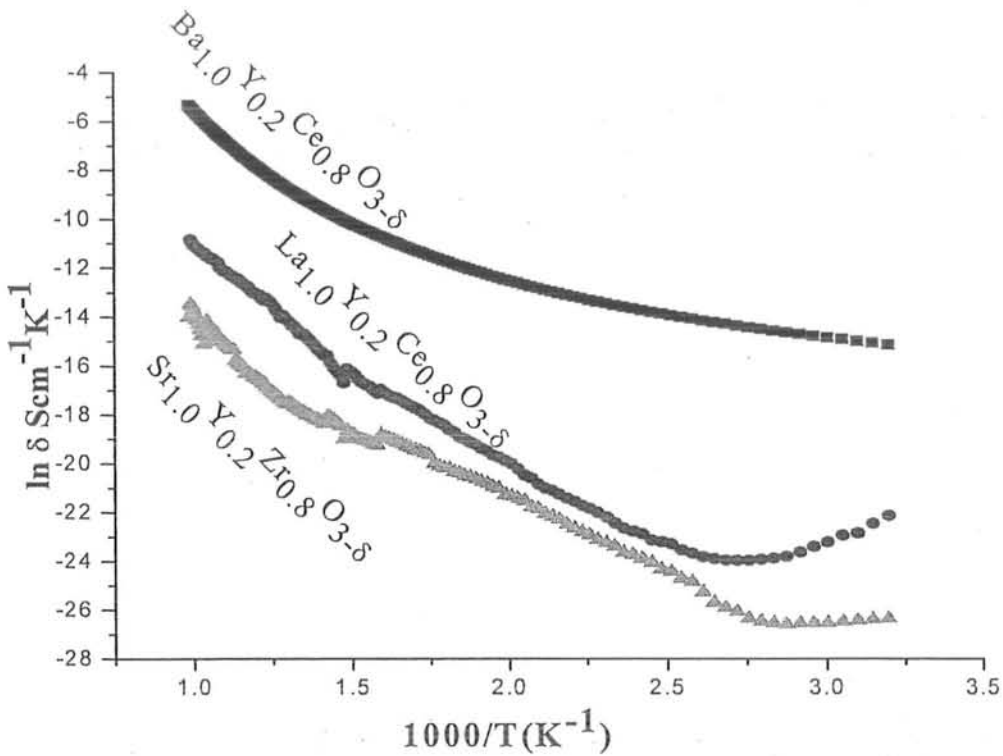
Figure 38: Comparison of the electrical conductivity of yttrium doped cerates and zirconates.

Comparison of the three electrolytes in above figure show that the conductivity order is $Ba_{1.0}Y_{0.2}Ce_{0.8}O_{3-\delta} > La_{1.0}Y_{0.2}Ce_{0.8}O_{3-\delta} > Sr_{1.0}Y_{0.2}Zr_{0.8}O_{3-\delta}$. This order indicate that yttrium doped cerates have higher conductivity than that of zirconates. All these electrolytes are oxygen deficient containing oxygen vacancies ($V_O^{\bullet\bullet}$). These oxygen vacancies are produced when metal at B site is doped with the another metal of lower oxidation state e.g. in above electrolytes the Ce(IV) or Zr(IV) is doped with the Y(III). The element in oxidation state of +4 can accommodate two oxygen atoms but 1.5 oxygen atoms can reside with the metal having oxidation state of +3. Thus oxygen vacancies are produced at the place where doping takes place. The presence of oxygen vacancies are necessary for an electrolyte to show the proton conductivity. Under moist conditions the proton defects are produced in the electrolyte by the chemical diffusion of water. Water split into hydroxide ions and protons, hydroxide ion occupy the oxygen

vacant site and proton get attach to the structural oxygen. Thus two proton defects are produced by splitting one water molecule. The protons which are attach to the oxygen show a rotational diffusion through the electrolyte. Hence under moist conditions the conductivity of the electrolytes is due to the motion of these hydrogen bonded protons. When the environment is dry and water is not available for the formation of proton defects then the oxide ions and holes contribute much in the electrical conductivity of these electrolytes. Oxygen from the air is absorbed into the oxygen vacant sites and is accompanied with the formation of electron holes as shown by the equation.

$$V_O^{\bullet\bullet} \;+\; 1/2 O_2 \;\rightleftharpoons\; O_O^X \;+\; 2h^{\bullet}$$

Thus the electrical conductivity of electrolytes depends upon the ease of motion of oxide ions in dry conditions. Cerates posses high conductivity than zirconates as shown in the Fig 38. It means that cerates have relatively loose oxide ions than zirconates. The motion of oxide ions is affected by the metals at site A and Site B. The zirconium has high electronegativity than that of cerium, therefore the Zr-O bond is less polar as compare to that of Ce-O bond. In other words Ce has high basicity than zirconium[75]. When the electric potential is provided across the electrolyte membrane the more polar oxide ions skip easily from the structure and move across the bulk. Ionic radius of Zr (IV) is 72pm while that of Ce (IV) is 87pm. Thus the zirconium has greater charge density than cerium and forms a strong bond with oxygen than that of cerium. Thus Zr-O bond is shorter as compare to Ce-O bond. This is also indicated by the FT-IR spectrum that Zr-O bond show stretching vibrations at higher frequency than Ce-O bond. Thus oxygen ions are trapped more in the zirconates and require greater energy to move, while in cerates the oxide ions are relatively free and have low activation energy, thus oxide ions move faster in cerates than in zirconates. Thus cerates show high conductivity as compare to zirconates. Cerates show high proton conductivity when the wet hydrogen is available [76]. The ionic radius and charge density of B site metal is also responsible for such kind of behavior. When protons from outside environment get attach to the structural oxygen ,the M-O bond length is increased because of two factors, interaction of the oxygen atom with that of the proton will result in decreasing the interaction of oxygen with metal atom which result in M-O bond lengthing, positively charged proton is repelled by the metal atom which also result in

M-O bond lengthning.Thus proton experiences two types of forces within the perovskite structure. Attractive forces from the oxide ions and repulsive forces from the positively charged metal atoms. Due to this repulsion between the proton and metal atom the O-H···O bond in the octahedron become bent and this orientation of proton will offer an energy barrier in rotational diffusion of proton from one oxygen atom to the next. Greater the charge on the metal atom greater will be the repulsion between metal and proton and O-H···O bond will be more bent and hence the activation energy for proton motion will be high.

Zr(IV) has greater charge density as compare to that of Ce(IV) therefore the Zr/H repulsion is high as compare to Ce/H. thus the O-H···O bond is more linear in cerates than in zirconates and can undergo faster rotational diffusion in the former. Therefore the proton conductivity is high in the cerates than in the zirconates under humid conditions and under dry conditions the oxide conduction is also high in cerates than in zirconates.
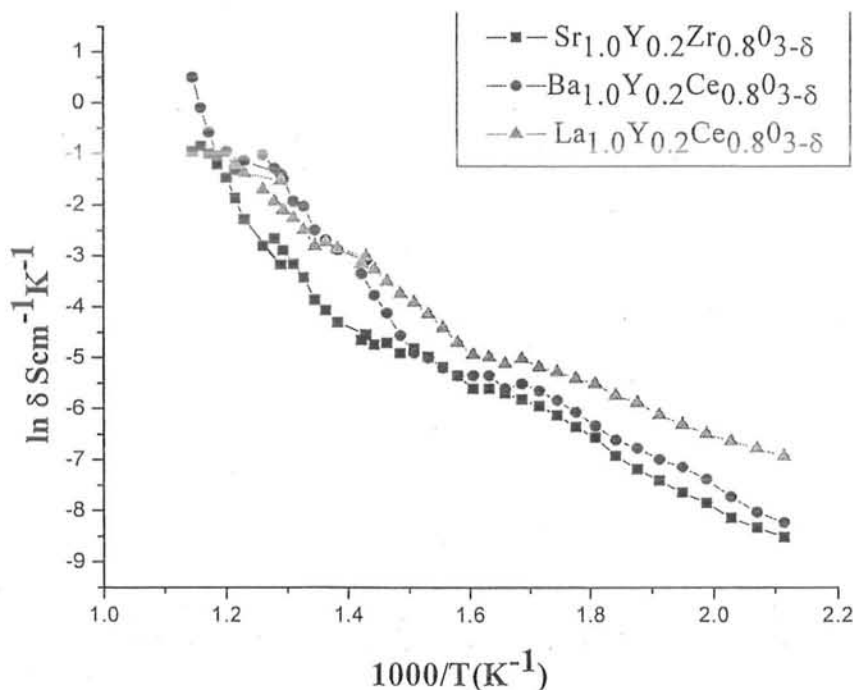

Figure 39: Comparison of the electrical conductivities of cerates and zirconates in moist air at T=300-600°C

Metal present at the A site also affect the oxide ion and proton conductivity of the electrolyte membrane e.g. the electrical conductivityof $Ba_{1.0}Y_{0.2}Ce_{0.8}O_{3-\delta}$ is high as compare to that of $La_{1.0}Y_{0.2}Ce_{0.8}O_{3-\delta}$ as shown in the Fig 4. The difference lies only at the A site metals. Barium has ionic radius of 135pm and valence state of +2 while Lanthanum has ionic radius and valence state 103.2pm and +3 respectively. Thus lanthanum has greater charge density than that that of Barium. As the metal present at site A has coordination number 12, i.e. it is attached to 12 oxygen atoms. The oxygen atoms are bound strongly with the Lanthanum than that of the Barium and hence the oxygen atoms are loose in the $Ba_{1.0}Y_{0.2}Ce_{0.8}O_{3-\delta}$ as compare to $La_{1.0}Y_{0.2}Ce_{0.8}O_{3-\delta}$. Therefore the former electrolyte show high oxide ion conductivity in dry conditions at high temperature.

Conductivities of $La_{1.0}Y_{0.2}Ce_{0.8}O_{3-\delta}$, $Ba_{1.0}Y_{0.2}Ce_{0.8}O_{3-\delta}$ and $Sr_{1.0}Y_{0.2}Zr_{0.8}O_{3-\delta}$ in moist air show a comparable behavior as shown in the Fig. 39. The conductivity of the $Ba_{1.0}Y_{0.2}Ce_{0.8}O_{3-\delta}$ is higher as compare to rest of the electrolyte membranes at high temperature. At 600°C the conductivity of the $La_{1.0}Y_{0.2}Ce_{0.8}O_{3-\delta}$ and $Sr_{1.0}Y_{0.2}Zr_{0.8}O_{3-\delta}$ are almost same as shown in the upper portion of the graph.

The high conductivity of the electrolyte membranes under moist air conditions make them appropriate materials to use as electrolyte for the intermediate temperature proton conducting solid oxide fuel cells.

CONCLUSION

Three types of the trimetallic oxide ceramic materials i.e (1) $La_{1.0}Ce_{0.8}Y_{0.2}O_{3-\delta}$,(2) $Ba_{1.0}Ce_{0.8}Y_{0.2}O_{3-\delta}$,(3) $Sr_{1.0}Zr_{0.8}Y_{0.2}O_{3-\delta}$, are synthesized successfully using the solution method and characterized by the different analytical techniques such as XRD, Thermogravimetry (TGA), FT-IR, EDX, SEM and electrical conductivity.

The material formed were analyzes using the X-Ray diffraction for their phase purity and it was found that all the materials were single phase having XRD spectra matching with the standard peak patterns. The particle size was also determined from the XRD pattern using the Scherrer,s formula. All materials were found in nano size range. The elemental ratio was calculated by using the EDX and surface morphology was determined by the SEM micrographs.

The requirement for the electrolyte ceramic materials to show the proton conductivity is the presence of oxygen vacant sites and proton defects. The oxygen vacant sites in the electrolyte membranes were estimated by using the TGA analysis and FT-IR spectroscopy confirmed the presence of proton defects.

The electrical conductivity of electrolyte ceramic materials was evaluated in dry air and moist air as a function of temperature using the Keithley electrical conductivity meter. Proton conductivity in moist air was much higher than electron hole and oxide ion conductivity in dry air at 600°C. Because of efficient proton conductivity, these materials can be used for the different technological applications such as electrolyte for the high temperature proton conducting solid oxide fuel cells, Galvanic cell type hydrogen sensors, steam sensors, hydrocarbon sensors and solid electrolyte diaphragm for hydrogen extraction.

REFERANCES

[1]   Martin,F.H.B. Perovskite type ceramic membranes.PhD thesis.University of Twente.**2005**,1

[2]   Muller O., and Roy R. The Major Ternary Structural Families. *Crystal chemistry of non-metallic materials*.**1974**, 1, 10

[3]   Woodward, P.M.; *Acta. Cryst.* **1997**, *B53*, 32-43.

[4]   Goldschmidt V.M., Skrifer Norske Videnskaps-Akad. Oslo, I. Mat.-Nat. Kl. **1926**, 8

[5]   Anthony.R.West, "*Basic Solid State Chemistry*", J.W& D. Ltd. **1999**, 55,364.

[6]   Batteries, Supercapacitors, and Fuel Cells: Scope". Science Reference Services.**2007**,17-3

[7]   Tsiakaras P., Demin A., *J. Power Sources.* **2001**, 102,210.

[8]   Douvartzides S. L., Countelieris F. A., Tsiakaras P. E., *J. Power Sources* .**2003**, 114,203

[9]   Yi Y. F., Rao A. D., Brouwer J., Samuelsen G. S., *J. Power Sources.* **2005**, 144, 67.

[10]   Gupta G. K., Hecht E. S., Zhu H. Y., Dean A. M., Kee R. J., *J. Power Sources* .**2006**, 156, 434.

[11]   Wojcik A., Middleton H., Damopoulos I., Van herle J., *J. Power Sources* **2003**, 118, 342.

[12]   Trembly J. P., Marquez A. I., Ohrn T. R., Bayless D. J., *J. Power Sources.* **2006**, 158, 263.

[13]   Song T. W., Sohn J. L., Kim T. S., Ro S. T., *J. Power Sources.* **2006**, 158, 361.

[14]   Stiller C., Thorud B., Bolland O., Kandepu R., Imsland L., *J. Power Sources.* **2006**, 158, 303.

[15]   Calise F., Palombo A., Vanoli L., *J. Power Sources.* **2006**, 158, 225.

[16]   Araki T., Ohba T., Takezawa S., Onda K., Sakaki Y., *J. Power Sources.* **2006**, 158, 52.

[17]   Dah PI, Haugsru R, Lein HL, Grande T, Norby T, Einarsrud MA, *J Eur Ceram Soc.* **2007**, 27:4461.

[18]   Kreuer K.D., *Chem. Mater.* **1996**, 8, 610.

[19] Kreuer K.D., Weppner W., Rabenau A., *Solid State Ionics* .**1981**, 3/4, 353.

[20] Kreuer K.D., Rabenau A., Weppner W., *Angew. Chem. Int. Ed. Engl.***1982**, 21, 208.

[21] Fischer S.F., Hofacker G.G., Ratner M.M., *J. Chem. Phys.* **1970**, 52, 1934.

[22] Marcus R.A., *J. Chem. Phys.* **1956**, 24, 966.

[23] Flynn C.P., Stoneham A.A., *Phys. Rev.***1970**, 1, 3966.

[24] Tuckerman M.E., Marx D., Klein M.M., Parrinello M., *J. Chem. Phys.* **1995**, 103, 45.

[25] Agmon N., *Chem. Phys. Lett.* **1995**, 244, 456.

[26] Kreuer K.D., *Solid State Ionics.* **2000**, 136, 149.

[27] K.D. Kreuer., W. Mu¨nch., M. Ise, A. Fuchs, U. Traub, J. Maier, Ber. Bunsenges. *Phys.Chem.* **1997**, 101, 1344.

[28] Murugaraj P., Kreuer K.D., He T.,. Schober T, Maier J., *Solid State Ionics.* **1997**, 98, 1.

[29] Sata N., Shin S., Shibata K., Ishigame M., J., *Phys. Soc. Jpn.* **1999**, 68, 3600.

[30] Shimojo F., Hoshino K., Okazaki H., *Solid State Ionics.* **1998**, 113, 319.

[31] Shimojo F., Hoshino K., *Solid State Ionics.* **2001**, 145, 421.

[32] Munch W., Seifert G., Kreuer K.K, Maier J., *Solid State Ionics.* **1996**, 86-88,647.

[33] Munch W., Kreuer K.K., Seifert G., Maier J., *Solid State Ionics.* **1999**, 125, 39.

[34] Seifert, J. Maier, *Solid State Ionics.* **2000**,183, 136.

[35] Kreuer K.D., Mu¨nch W., Traub U., Maier J., *Phys. Chem.* **1998**   102, 552.

[36] Matzke, T., Stimming, U., Karmonik, C., Soetramo, M., Hempelmann, R., Gu¨ thoff, F., *Solid State Ionics.* **1996**, 86, 621.

[37] Hempelmann, R., Soetramo, M., Hartmann, O., Wa¨ppling, R., *Solid State Ionics.***1998**, 107, 269.

[38] Iwahara, H., *Solid State Ionics.***1996**, 86, 9.

[39] Kreuer, K.D., Proton conducting oxides. *Annu Rev Mater Res.* **2003**, 33,333.

[40] Kreuer, K.D., Proton-Conducting Oxides, *Annu. Rev. Mater. Res.* **2003**,59.

[41] Munch ,W., Seifert, G., Kreuer, K.K, Maier, J., *Solid State Ionics.* **1996**, 86, 647.

[42] Munch, W., Kreuer, K.K., Seifert, G., Maier, J., *Solid State Ionics* .**2000**,136, 183

[43] Murugaraj, P., Kreuer, K.K., He, T., Schober, T., Maier, J., *Solid State Ionics.* **1997**, 98, 1.

[44] Munch, W., Kreuer, K.K., Seifert, G., Maier, J., *Solid State Ionics.* **1999**, 125, 39.

[45] Kreuer K.D., *Solid State Ionics.* **2000,** 136–137, 149.

[46] Mu¨ nch, W., Seifert, G., Kreuer, K.K, Maier, J., *Solid State Ionics* .**1996**, 86, 647.

[47] Kreuer, K.D., Proton-Conducting Oxides. *Annu.Rev. Mater. Res.* **2003**, 33, 335.

[48] Munch, W., Kreuer, K.D., Adams, St., Seifert, G., Maier, J., *Phase Transitions* . **1999**,68,332.

[49] Kreuer, K.D., Munch, W., Traub, U., Maier, J., Ber. Bunsenges. *J.Phys. Chem.* **1998,** 102, 552.

[50] Kreuer K.D., *Solid State Ionics.* **1999**, 125, 285.

[51] Kreuer, K.D., Adams, S., Fuchs, A., Klock, U., Mu¨ nch, W., Maier, J., *Solid State Ionics.* **2001**, 145, 295.

[52] M¨unch, W., Kreuer, K.D., Adams, S., Seifert, G., Maier, J,. *Phase Transitions.* **1999**, 68, 567.

[53] Dah, PI., Haugsru, R., Lein, H.L., Grande, T., Norby, T., Einarsrud, M.A., *J Eur Ceram Soc.* **2007**, 27,4461

[54] Iwahara, H., *Solid State Ionics.* **1996**, 86,9.

[55] Iwahara, H. *Solid State Ionics.* **1995**, 77,289.

[56] Xueqing Sha., Zhe Lü., Xiqiang Huang., Jipeng Miao., Zhanhui Ding., Xianshuang Xin., and Wenhui Su. *'Study on La and Y co-doped ceria-based electrolyte materials'.* J alloys and compounds. **2007**, 428,59.

[57] Lu, E. C., Iglesia, E., Synthesis of yttria-doped strontium-zirconium oxide powders via ammonium glycolate, *J of mater sci,* **2001,** 36,77.

[58] Sha, X., Lu, Z., Huang, X., Miao, J., Ding, Z., Xin, Z., Su, W., Study on La co doped ceria-based electrolyte materials,*J alloys and compounds.* **2007** ,428,59

[59] Keruer, K.D.,. *Solid State Ionics.* **1999**, 125,302.

[60] Bonanos, N., *Solid State Ionics* .**1992**, 53, 967.

[61]   He, T., Kreuer, K.D., Maier J. *Solid State Ionics.* **1997**, 95,301.

[62]   He T,Kreuer KD, Baikov YM, Maier *J. Proc. Electrochem. Soc.* **1997**, 97,1057.

[63]   Phair, J. W., Badwal, S. P. S., *Review of proton conductors for hydrogen separation.* **2006**,12,110.

[64]   Kim, D.J. *J. Am. Ceram. Soc.* **1989**, 72,1415.

[65]   Inaba, H., Tagawa, H. *Solid State Ionics.* **1996**, 83,16.

[66]   Mickael, P., Jeremy, B., Aude, M., Jean-Francois, H. Effect of hydrothermal ripening on the photoluminescence properties of pure and doped cerium oxide nanoparticles, *J. meter. Chem. & Phy.***2010**, 120,79

[67]   Bakar, S.N.A., Talib, I.A., and Osman, N., , *J.solid state science and tech.* **2009**, 17, 25.

[68]   Keruer, K.D.,. *Solid StatIonics.* **1997**, 97, 1.

[69]   Keruer, K.D.,. *Annual review of material research.* **2003**, 33, 334.

[70]   Tatsumi., Ishihara. Perovskite oxides for the solid oxide fuel cells. *Solid StatIonics.* **2008**, 246,1.

[71]   Koshy, J., Jose, R., Asha, M.J., James, J., *Council of Scientific & IndustrialResearch Trivandrum, India., Private Communication,* **1999.**

[72]   Lefebvre-Joud, F., Gauthier, G., Mougin, J.,Current status of proton-conducting solid oxide fuel cells development. *J. Appl. electronics.***2009**, 39, 538.

[73]   Perovskite oxides for the solid oxide fuel cells. Springer Dordrecht Heidelberg London New York.**2008**; Vol.1,p. 243.

[74]   Bakar, S.N.A., Talib, I.A., and Osman, N. *Solid State Science and Technology* **2009,** 17, 25.

[75]   Fuel cells and hydrogen energy. Springer Dordrecht Heidelberg London New York.**2008**; Vol.1,p. 246.

[76]   Norby, T., Larring, Y. *curr.open. solid State Mater. Sci.***1997**, 2, 593.